arXiv:2611.09878v1 [cs.CV] 6 Nov 2026

GRADED CONVOLUTIONAL NETWORKS: SCALE INVARIANCE WITHOUT THE SCALE AND ROBUSTNESS TO UNKNOWN BLUR

T. SHASKA

Abstract. The Gaussian jet of an image is a graded vector space: a dilation by λ multiplies derivatives of order k by λ^{-k}. Local graded convolutions are exactly homogeneous differential operators, and a local feature is dilation-invariant if and only if it factors through the scale-normalized jet or, without the scale, through the retraction onto the weighted sphere of the grading. Under unknown Gaussian blur the retraction changes only by a change of scale, whereas the scale-normalized jet acquires a grading factor that no radial normalization removes. At the zero jet the retraction separates image families that radial normalizations and continuous classifiers cannot. Networks built on the retraction are universal for invariant features. On MNIST such a network keeps 88.4% accuracy under a two-pixel blur, against 66.2% for the same network on scale-normalized derivatives; in Lindeberg's Gaussian derivative network the retraction raises accuracy at that blur from 91.5% to 95.1%.

1. Introduction

Let I be an image on $\mathbb{R}^2$ and $L(x;s) = (g_s * I)(x)$ its Gaussian scale space. The derivatives of order k of L at $(x;s)$ are the coefficients of a binary form f_k of degree k, and the jet $f = (f_1, \dots, f_N)$ lies in the graded vector space $V^+ = \bigoplus_{k=1}^{N} \operatorname{Sym}^k(\mathbb{R}^2)^*$. A magnification of the image by $\lambda > 0$ carries the jet at $(x;s)$ to the jet $\lambda^{-1} \star f$ at $(\lambda x; \lambda^2 s)$, where $\mu \star f = (\mu^k f_k)_k$ is the grading action of the multiplicative group [1–3]. Every network that reads an image through its Gaussian jets carries this action, from the Gaussian derivative networks of Lindeberg [9, 10, 24, 25] to the networks on harmonic coordinates [26, 27]. We determine the local features that are invariant under it, and what such features give a classifier.

Two maps organize the answer. The *scale-normalized jet* $\nu(f,s) = s^{1/2} \star f$ uses the smoothing scale; it is the γ-normalization of [11] with $\gamma = 1$. The *graded retraction*

$$\pi_{\mathbf{q}}(f) = \Big(\frac{f_k}{\rho_{\mathbf{q}}(f)^k} \Big)_{k=1}^{N}, \qquad \rho_{\mathbf{q}}(f) = \Big(\sum_{k=1}^{N} \|f_k\|^{2/k} \Big)^{1/2},$$

maps $V^+ \smallsetminus 0$ onto the weighted sphere $S_{\mathbf{q}} = \{\rho_{\mathbf{q}} = 1\}$ along the orbits of the grading action and does not use the scale.

Theorem A. *A continuous linear operator between graded fields on $\mathbb{R}^2$ that commutes with translations and dilations and does not enlarge supports is a homogeneous differential operator with constant coefficients whose order is the shift of grade. In particular the N-jet is the universal local graded convolution of order at most N.*

Theorem B. *Let $\lambda > 0$ act on pairs (f,s) of a jet and a scale by $\lambda \cdot (f,s) = (\lambda^{-1} \star f, \lambda^2 s)$. A map $\Phi(f,s)$ is invariant if and only if it factors through ν, and a map $\Psi(f)$ that does not depend on s is invariant if and only if it factors through $\pi_{\mathbf{q}}$. For weights $\boldsymbol{\theta}$ other than the derivative orders*

Date: November 9, 2026.

2020 *Mathematics Subject Classification.* Primary 68T07, 13A50; Secondary 68U10, 14L24, 15A72, 46F10.

Key words and phrases. graded vector spaces, scale space, scale invariance, Gaussian blur, invariant theory, equivariant neural networks.

$\mathbf{q} = (1, \dots, N)$ *the normalization* $(s^{\theta_k/2} f_k)_k$ *is not invariant, and the retraction onto the weighted sphere of* $\boldsymbol{\theta}$ *is invariant if and only if* $\boldsymbol{\theta}$ *is proportional to* $\mathbf{q}$.

Theorem C. *Let* $b > 0$ *and* $I' = g_b * I$. *Then* $f^{I'}(x; s) = f^I(x; s + b)$, *so that*

$$\pi_{\mathbf{q}}\big(f^{I'}(x;s)\big) = \pi_{\mathbf{q}}\big(f^I(x; s+b)\big), \qquad \nu\big(f^{I'}(x;s), s\big) = \mu \star \nu\big(f^I(x;s+b), s+b\big), \quad \mu = \Big(\frac{s}{s+b}\Big)^{1/2},$$

and the radial projection of $\mu \star u$ *differs from that of* u *unless all nonzero blocks of* u *have the same order.*

An unknown blur thus acts on the retraction by a change of scale alone, which a network evaluated on a ladder of scales encounters in training, and on the normalized jet by an additional grading factor that no radial normalization removes.

The retraction is smooth where all blocks of the jet are nonzero and Hölder continuous on $V^+ \smallsetminus 0$, but it has no continuous extension to the zero jet. At this singular point the graded quotient resolves local structure that radial normalizations, and classifiers continuous in the image, do not.

Theorem D. *There are smooth images* $I_t^{\pm}$, $0 < t < t_0$, *converging uniformly to one image as* $t \to 0$, *with the same intensity mass and frame and the same Gaussian jets at all probes but one, where the jets are* $(tu_1, \pm t^2 u_2, 0)$, *with the following properties. Some probe classifier built on* $\pi_{\mathbf{q}}$ *takes the values* ± 1 *on* $I_t^{\pm}$ *for every* t. *Every probe classifier built on the radial projection of the raw or of the scale-normalized jet, and every classifier continuous at the limit image, has worst-case squared loss at least* 1 *on the family. With a fixed regularization of* $\rho_{\mathbf{q}}$ *the graded probe classifiers have worst-case squared loss* 1 *as well.*

These results determine an architecture, the graded convolutional network of Sec. 6: Gaussian jets on a geometric ladder of scales, the retraction $\pi_{\mathbf{q}}$, layers equivariant under rotations that act on harmonic coordinates by complex-linear maps, products and gates, and a pooling over positions and scales in a frame of the image that is covariant under dilations and translations. Its pooled features are invariant under the dilations by powers of two, and it is universal for continuous invariant functions on the quotient (Thm. 6.6). Along a scale orbit, on which a ReLU network on the raw jet diverges polynomially and a network on its radial projection collapses onto a single derivative order, it is constant (Thm. 6.8).

Sec. 8 tests Theorem B and Theorem C on MNIST, against networks that differ from the graded one only in the normalization of the jet. Trained on sharp digits at one scale, the graded network keeps at least 92% accuracy over a fourfold range of zoom in each of three training splits, while the same network with equal grades loses up to 41 points. Under a Gaussian blur of two pixels it keeps 88.4%, against 66.2% for the same network on scale-normalized derivatives, and exchanging the foreground gates of the graded network and its equal-grades twin shows that the retraction, not the gate, carries this robustness; on sharp images the scale-normalized network is about one point more accurate. In Lindeberg's Gaussian derivative network, retracting the jet of the first layer and changing nothing else raises the accuracy at a blur of two pixels from 91.5% to 95.1%, and a graded first layer improves a second version of that network as well.

The jet has represented local image structure since Koenderink [6–8], and blurring and scaling as operators on jet space were studied by Markussen, Pedersen and Loog [22, 23]. Theorem A is a specialization of the distribution theory of homogeneous kernels [4]; equivariant differential operators for rotations and Euclidean motions were characterized by Jenner and Weiler [26]. Complex features labelled by a rotation frequency and combined by products that add the frequencies are the charge-conserving networks of Yarotsky [27], who proved their universality; the layers of the graded network are of this kind, with the derivative order as a second label. Scale-equivariant networks with learned filters [18–20] also carry a ladder of scales. Exact invariants to an unknown Gaussian blur, and to wider families of convolutions, have been constructed from image moments and projection operators by Flusser and coauthors [28–30]. The graded retraction is not such an invariant (Sec. 5.1); our concern is how a scale-invariant representation responds to blur.

Sec. 2 introduces graded jets, homogeneous norms and weighted spheres, and the space of local structures. Theorem A is proved in Sec. 3, Theorem B in Sec. 4 and Theorem C in Sec. 5, which also treats the passage between scales. Sec. 6 defines the graded networks and proves their invariance and universality, Sec. 7 proves Theorem D, and Sec. 8 reports the experiments. The appendix describes the discretization and its numerical verification. The code, the trained networks and the result files from which every table and figure is generated are deposited on Zenodo [34].

2. Graded jets

In Secs. 2 to 7 images are functions on the plane, derivatives are exact Gaussian derivatives, and the homogeneous norm is unregularized except in Thm. 7.7.

2.1. **Scale space and jets.** Derivatives of an image are taken after smoothing with the Gaussian $g_s(x) = (2\pi s)^{-1}\exp(-|x|^2/2s)$, which is not homogeneous but covariant, $g_s * (D_\lambda I) = D_\lambda(g_{s/\lambda^2} * I)$, where $(D_\lambda I)(x) = I(x/\lambda)$ is the magnification by λ. Write $L(x;s) = (g_s * I)(x)$, $L_\alpha = \partial^\alpha L$, and collect the derivatives of order k into the binary form

$$f_k(\xi,\eta;x,s) = \sum_{a+b=k} \binom{k}{a} L_{(a,b)}(x;s)\,\xi^a\eta^b \in V_k = \mathrm{Sym}^k(\mathbb{R}^2)^*, \tag{1}$$

so that $L(x+h;s) = \sum_k f_k(h)/k!$ formally. The N-jet is $f = (f_0,\dots,f_N) \in V = \bigoplus_{k\le N} V_k$, with $\dim V_k = k+1$ and $\dim V = \frac{(N+1)(N+2)}{2}$; for $N=3$, $\dim V = 10$, f_1 is the gradient, f_2 the Hessian form and f_3 a binary cubic. The grading action is $\mu \star f = (\mu^k f_k)_k$.

Lemma 2.1. *For every $\lambda > 0$, $x \in \mathbb{R}^2$ and $s > 0$,*

$$f^{D_\lambda I}(x;s) = \lambda^{-1} \star f^I(x/\lambda;\, s/\lambda^2). \tag{2}$$

Consequently the normalized jet $\tilde f(x;s) = s^{1/2} \star f(x;s)$, that is $\tilde f_k = s^{k/2} f_k$, satisfies $\tilde f^{D_\lambda I}(x;s) = \tilde f^I(x/\lambda; s/\lambda^2)$.

Proof. By the covariance of the Gaussian and the chain rule, $L_\alpha^{D_\lambda I}(x;s) = \lambda^{-|\alpha|} L_\alpha^I(x/\lambda; s/\lambda^2)$. For the second statement, $s^{1/2} \star \lambda^{-1} \star = (s/\lambda^2)^{1/2} \star$. □

The scale s is thus a homogeneous function of degree two on the bundle of jets, and $\tilde f = \sqrt{s} \star f$ is the normalization of the jet by the homogeneous function $\sqrt{s}$ of degree one. This is the γ-normalization of [11] with $\gamma = 1$; Thm. 4.1 shows that the exponent is forced.

2.2. **Harmonic coordinates.** Rotations $R \in \mathrm{SO}(2)$ act on images by $(R\cdot I)(x) = I(R^{-1}x)$ and on the jet by $f_k \mapsto f_k \circ R^{-1}$, the restriction to $\mathrm{SO}(2)$ of the action of GL_2 on binary forms; they commute with dilations. Under $\mathrm{SO}(2)$,

$$V_k = \mathcal{H}_k \oplus (\xi^2+\eta^2)\mathcal{H}_{k-2} \oplus \cdots, \tag{3}$$

where $\mathcal{H}_j$, the harmonic forms of degree j, is the irreducible representation of frequency j, of dimension 2 for $j \ge 1$ and 1 for $j = 0$; this is the decomposition behind steerable filters [12, 17]. In the complex coordinate $z = \xi + i\eta$ write $f_k = \sum_{a+b=k} c_{k,b-a}\, z^a \bar z^b$, with $c_{k,-j} = \bar c_{k,j}$. The rotation by ϕ sends $z \mapsto e^{-i\phi} z$ and $\bar z \mapsto e^{i\phi}\bar z$, so

$$c_{k,j} \mapsto e^{ij\phi} c_{k,j}, \qquad j = k, k-2, \dots,\ j \ge 0. \tag{4}$$

The *harmonic coordinates* $c_{k,j}$, $j \ge 0$, are complex numbers, real for $j = 0$, on which $\mathrm{SO}(2)$ acts diagonally by the frequency j and the grading action by μ^k. For $N = 3$ there are five of them, of order and frequency $(1,1)$, $(2,0)$, $(2,2)$, $(3,1)$ and $(3,3)$. For the 2-jet they are, up to factors, the classical complex coordinates

$$z_1 = L_x + iL_y, \qquad h_0 = \tfrac12(L_{xx}+L_{yy}), \qquad h_2 = \tfrac12(L_{xx}-L_{yy}) + iL_{xy},$$

which are twice the coefficient of $\bar z$ in f_1, the coefficient of $z\bar z$ in f_2 and twice the coefficient of $\bar z^2$ in f_2. The classical differential invariants of second order are polynomials of frequency zero in them: $|\nabla L|^2 = z_1\bar z_1$, $\Delta L = 2h_0$, $\det \mathrm{Hess}\, L = h_0^2 - h_2\bar h_2$ and $\nabla L^\top \mathrm{Hess}\, L\, \nabla L = h_0 z_1 \bar z_1 + \mathrm{Re}(\bar h_2 z_1^2)$.

2.3. **Homogeneous norms and weighted spheres.** Let $\boldsymbol{\theta} = (\theta_1, \dots, \theta_N)$, $\theta_k > 0$, be a vector of grades with the action $\mu \star_{\boldsymbol{\theta}} f = (\mu^{\theta_k} f_k)_k$ on $V^+ = \bigoplus_{k=1}^N V_k$, and let $\|f_k\|$ be an $\mathrm{SO}(2)$-invariant norm on V_k; we use the Euclidean norm of the harmonic coordinates. Define

$$\rho_{\boldsymbol{\theta}}(f) = \Big(\sum_{k=1}^{N} \|f_k\|^{2/\theta_k}\Big)^{1/2}, \qquad \pi_{\boldsymbol{\theta}}(f)_k = \frac{f_k}{\rho_{\boldsymbol{\theta}}(f)^{\theta_k}}. \tag{5}$$

Lemma 2.2. *$\rho_{\boldsymbol{\theta}}$ is continuous on V^+, positive off 0, $\mathrm{SO}(2)$-invariant and homogeneous of degree one, $\rho_{\boldsymbol{\theta}}(\mu \star_{\boldsymbol{\theta}} f) = \mu \rho_{\boldsymbol{\theta}}(f)$. The weighted sphere $S_{\boldsymbol{\theta}} = \{\rho_{\boldsymbol{\theta}} = 1\}$ is compact, and $\pi_{\boldsymbol{\theta}}$ is a continuous retraction of $V^+ \smallsetminus 0$ onto $S_{\boldsymbol{\theta}}$ that is constant along the orbits of $\star_{\boldsymbol{\theta}}$. For $\boldsymbol{\theta} = (1, \dots, 1)$, $\rho_{\boldsymbol{\theta}}$ is the Euclidean norm and $\pi_{\boldsymbol{\theta}}$ the radial projection.*

Proof. $\|\mu^{\theta_k} f_k\|^{2/\theta_k} = \mu^2 \|f_k\|^{2/\theta_k}$, and $\pi_{\boldsymbol{\theta}}(\mu \star_{\boldsymbol{\theta}} f)_k = \mu^{\theta_k} f_k / (\mu \rho_{\boldsymbol{\theta}}(f))^{\theta_k}$. □

This is the homogeneous norm of [1], written with the exponents $2/\theta_k$ so that it is defined for real grades. The grades of the image jet are $\mathbf{q} = (1, 2, \dots, N)$, and $\pi_{\mathbf{q}}$ is the quotient map of $V^+ \smallsetminus 0$ by the grading action. We write $\pi_{\mathbf{1}}$ for the radial projection. By Thm. 2.1, $\rho_{\mathbf{q}}(\tilde{f}) = s^{1/2} \rho_{\mathbf{q}}(f)$ and $\pi_{\mathbf{q}}(\tilde{f}) = \pi_{\mathbf{q}}(f)$: the retraction of the normalized jet is the retraction of the raw jet. The scalar $\tilde{\rho} = \rho_{\mathbf{q}}(\tilde{f})$ is invariant under dilations at the corresponding scale; it is a scale-normalized energy of the jet of the kind used for scale selection [11], and it is not invariant under contrast, $\rho_{\mathbf{q}}(cf)^2 = \sum_k c^{2/k} \|f_k\|^{2/k}$.

Lemma 2.3. *Let $N \geq 2$. The retraction $\pi_{\mathbf{q}}$ is smooth on the open set where every block f_k is nonzero and locally Hölder continuous of exponent $\min(1, 2/N)$ on $V^+ \smallsetminus 0$, and for $N \geq 3$ this exponent cannot be improved. It has no continuous extension to 0.*

Proof. The function $f_k \mapsto \|f_k\|^{2/k} = (\|f_k\|^2)^{1/k}$ is smooth where $f_k \neq 0$ and locally Hölder continuous of exponent $\min(1, 2/k)$ on V_k. Hence $\rho_{\mathbf{q}}^2$ is locally Hölder of exponent $\min(1, 2/N)$, and so is $\rho_{\mathbf{q}}^{-k} = (\rho_{\mathbf{q}}^2)^{-k/2}$ on every compact subset of $V^+ \smallsetminus 0$, where $\rho_{\mathbf{q}}$ is bounded below; the components $f_k \rho_{\mathbf{q}}^{-k}$ of $\pi_{\mathbf{q}}$ inherit both properties. For $N \geq 3$ let $u_1 \in V_1$ and $v \in V_N$ be unit vectors and $f_t = (u_1, 0, \dots, 0, tv)$. Then $\rho_{\mathbf{q}}(f_t)^2 = 1 + |t|^{2/N}$ and $\|\pi_{\mathbf{q}}(f_t)_1 - \pi_{\mathbf{q}}(f_0)_1\| = 1 - (1 + |t|^{2/N})^{-1/2} \sim \frac{1}{2}|t|^{2/N}$ as $t \to 0$. Finally, for unit vectors $u_1 \in V_1$ and $u_2 \in V_2$ the curves $t \mapsto (tu_1, \pm t^2 u_2, 0, \dots, 0)$ tend to 0 as $t \to 0$, while $\rho_{\mathbf{q}}^2 = 2t^2$ along both and their retractions are the constant points $(u_1/\sqrt{2}, \pm u_2/2, 0, \dots, 0)$. □

2.4. **The space of local structures.** Two further transformations change an image without changing what a recognizer should respond to: rotations, and the contrast changes $I \mapsto cI + d$ with $c > 0$, which act by $f_0 \mapsto cf_0 + d$ and $f_k \mapsto cf_k$ for $k \geq 1$. On V^+ the torus $T = \mathbb{G}_m \times \mathbb{G}_m$ of dilations and contrasts acts by $(\mu, c) \star f_k = \mu^k c\, f_k$, and $\mathrm{SO}(2)$ acts on each V_k and commutes with T. Let $G = T \times \mathrm{SO}(2)$.

Proposition 2.4. *For $N \geq 2$ the generic G-orbit on V^+ has dimension 3, so the space of N-jets modulo scale, rotation and contrast has dimension $\frac{(N+1)(N+2)}{2} - 4$: 2 for $N = 2$, 6 for $N = 3$ and 11 for $N = 4$.*

Proof. On the open dense set where $f_1 \neq 0$ and the trace component of f_2 is nonzero, let a, c and b be infinitesimal dilation, contrast and rotation parameters that fix f. In grade one, $(a + c) f_1 + b J f_1 = 0$, where J is the rotation by $\pi/2$; since $J f_1 \perp f_1$, $a + c = 0$ and $b = 0$. The trace component of grade two, on which rotations act trivially, gives $2a + c = 0$, hence $a = c = 0$. The infinitesimal stabilizer is zero, so the generic orbit has dimension three. □

The quotient of $V^+ \smallsetminus 0$ by the positive dilations is the weighted sphere $S_{\mathbf{q}}$, of dimension $\dim V^+ - 1$, which is 8 for $N = 3$. Its quotient by -1, acting by $(-1)^k$ on V_k, is the weighted projective space $\mathbb{P}(\mathbf{q}^+)$ with $\mathbf{q}^+ = (1, 1, 2, 2, 2, \dots, N^{(N+1)})$; since -1 acts as the rotation by π, the two coincide after the quotient by $\mathrm{SO}(2)$. We use positive dilations throughout.

Which of the three factors of G is a nuisance depends on the task. Scale is one throughout this paper. Contrast is removed at the input by $\hat{I} = (I - \min I)/(\max I - \min I)$, which commutes with dilations and rotations; a negative c, which gives $1 - \hat{I}$, is not removed, and constant images are mapped to

zero. Rotation is a nuisance for textures but not for upright digits, a 6 being a rotated 9; the networks of Sec. 6 are equivariant under rotations, and their readout decides whether the orientation is kept.

Remark 2.5. On the open set $\nabla L \neq 0$ the gauge coordinates $(L_w, L_{vv}, L_{vw}, L_{ww})$ of [8], taken in the frame $w = \nabla L/|\nabla L|$, $v = (-L_y, L_x)/|\nabla L|$, are rotation-invariant, with $L_w > 0$. In harmonic coordinates, with $u = \bar{h}_2 z_1^2/(z_1\bar{z}_1)$, one has $L_{ww} = h_0 + \operatorname{Re} u$, $L_{vv} = h_0 - \operatorname{Re} u$ and $L_{vw} = -\operatorname{Im} u$. Under $(\mu, c) \in T$ the coordinate L_w is multiplied by μc and the other three by $\mu^2 c$; with $\mu = L_w/|L_{ww}|$ and $c = |L_{ww}|/L_w^2$ a 2-jet is moved to $L_w = 1$, $L_{ww} = \pm 1$. Hence on the chart $L_{ww} \neq 0$ the ratios L_{vv}/L_{ww} and L_{vw}/L_{ww}, together with the sign of L_{ww}, separate the G-orbits of 2-jets, in accordance with Thm. 2.4. These coordinates fail where $\nabla L = 0$ or $L_{ww} = 0$. The retraction $\pi_{\mathbf{q}}$ is defined on all of $V^+ \smallsetminus 0$, and its only singular point, the zero jet, is the subject of Sec. 7.

3. Graded convolutions

Let $V = \bigoplus_{k=0}^N V_k$ be a graded real vector space. A *graded feature field* is a map $F = (F_0, \dots, F_N) : \mathbb{R}^2 \to V$. Translations act by $(T_a F)(x) = F(x - a)$, and dilations by

$$(D_\lambda F)_k(x) = \lambda^{-k} F_k(x/\lambda), \qquad \lambda > 0, \tag{6}$$

the change of variable of a magnification by λ combined with the grading action $\lambda^{-1}\star$ on the fibre [1]. An image $I : \mathbb{R}^2 \to \mathbb{R}$ is a field of grade 0, on which (6) is the magnification $(D_\lambda I)(x) = I(x/\lambda)$.

Definition 3.1. A *graded convolution* from grade k to grade k' is a continuous linear operator L from fields of grade k to fields of grade k' that commutes with all translations and all dilations, $LT_a = T_a L$ and $LD_\lambda = D_\lambda L$. It is *local* if $\operatorname{supp} LF \subseteq \operatorname{supp} F$ for every F.

Proposition 3.2. *Let $L : C_c^\infty(\mathbb{R}^2) \to \mathcal{D}'(\mathbb{R}^2)$ be a graded convolution from grade k to grade k'. Then $LF = K * F$ for a distribution K that is homogeneous of degree $k - k' - 2$. If L is local, then $k' \geq k$ and*

$$L = \sum_{|\alpha| = k' - k} c_\alpha \, \partial^\alpha,$$

a homogeneous differential operator of order $m = k' - k$ with constant coefficients. Conversely, every such operator is a local graded convolution from grade k to grade $k + m$.

Proof. A continuous linear operator on $C_c^\infty(\mathbb{R}^2)$ that commutes with translations is the convolution with a distribution K [4]. For the dilations compute, with $y = \lambda u$,

$$(K * D_\lambda F)(x) = \lambda^{-k} \int K(x - y) F(y/\lambda)\, dy = \lambda^{2-k} \int K(x - \lambda u) F(u)\, du,$$
$$(D_\lambda (K * F))(x) = \lambda^{-k'} \int K(x/\lambda - u) F(u)\, du.$$

Equality for all F gives, with $z = x/\lambda - u$, $K(\lambda z) = \lambda^{k - k' - 2} K(z)$ in the sense of distributions, so K is homogeneous of degree $k - k' - 2$. If L is local, then $\operatorname{supp} K = \{0\}$, and a distribution supported at a point is a finite sum $\sum_\alpha c_\alpha \partial^\alpha \delta$ [4]. Since $\partial^\alpha \delta$ is homogeneous of degree $-2 - |\alpha|$ and distributions of distinct degrees of homogeneity are linearly independent, $|\alpha| = k' - k$ whenever $c_\alpha \neq 0$; in particular $k' \geq k$. The converse is the chain rule, $\partial^\alpha (F(\cdot/\lambda)) = \lambda^{-|\alpha|} (\partial^\alpha F)(\cdot/\lambda)$. □

Corollary 3.3. *The N-jet map $I \mapsto (\partial^\alpha I)_{|\alpha| \leq N}$, with $\partial^\alpha I$ placed in grade $|\alpha|$, is a local graded convolution from grade 0 to $\bigoplus_{k \leq N} V_k$, and every local graded convolution from grade 0 of order at most N factors through it by a grade-preserving linear map.*

The map $I \mapsto f(\cdot; s)$ of Sec. 2.1 is this graded convolution applied to $g_s * I$; this proves Theorem A.

Remark 3.4. Without locality there are graded convolutions of grade shift zero other than the multiples of the identity. The distributions on $\mathbb{R}^2$ that are homogeneous of degree -2 are $c\,\delta + \text{p.v.}\, \Omega(z/|z|)/|z|^2$ with Ω of mean zero on the circle [4], and the singular integrals among them are nonlocal graded convolutions of grade shift zero. The Riesz transforms, with kernels $z_j/|z|^3$, which underlie the

monogenic signal [5], are of this kind. They could be added to the first layer, where their two components transform as a vector under rotations; we do not use them.

4. Invariants of the dilation action

Let $\mathbf{q} = (1, \dots, N)$. By Thm. 2.1 the dilation D_λ carries the jet f of I at $(x; s)$ to the jet $\lambda^{-1} \star f$ of $D_\lambda I$ at $(\lambda x; \lambda^2 s)$, so it acts on pairs of a jet and a scale by

$$\lambda \cdot (f, s) = (\lambda^{-1} \star f,\ \lambda^2 s), \qquad \lambda > 0. \tag{7}$$

A *local feature* is a map $\Phi : V^+ \times (0, \infty) \to Y$ into a set Y. It is *scale-invariant* if $\Phi(\lambda \cdot (f, s)) = \Phi(f, s)$ for all λ, f and s. Every element of V^+ is the jet at $(0; s)$ of an image in $C_c^\infty(\mathbb{R}^2)$: the map $I \mapsto f^I(0; s)$ is linear, and a linear form vanishing on its image would be a nonzero combination of derivatives of g_s orthogonal to every test function, which is impossible since these derivatives are linearly independent. Scale invariance of Φ is therefore equivalent to $\Phi\big(f^{D_\lambda I}(\lambda x; \lambda^2 s), \lambda^2 s\big) = \Phi\big(f^I(x; s), s\big)$ for all images, positions and scales. A feature that does not use the scale is a map $\Psi : V^+ \smallsetminus 0 \to Y$; it is scale-invariant if $\Psi(\lambda \star f) = \Psi(f)$ for all $\lambda > 0$.

For a vector $\boldsymbol{\theta}$ of positive weights let $\star_{\boldsymbol{\theta}}$, $\rho_{\boldsymbol{\theta}}$ and $\pi_{\boldsymbol{\theta}}$ be as in Sec. 2.3, and let

$$\nu_{\boldsymbol{\theta}}(f, s) = s^{1/2} \star_{\boldsymbol{\theta}} f = (s^{\theta_k/2} f_k)_k, \qquad \nu = \nu_{\mathbf{q}},$$

so that $\nu(f, s) = \tilde{f}$ is the normalized jet of Thm. 2.1. Lindeberg's γ-normalized derivatives [11] form $\nu_{\gamma\mathbf{q}}$.

Theorem 4.1. *(i) A local feature Φ is scale-invariant if and only if $\Phi = \Phi_0 \circ \nu$ for a map $\Phi_0 : V^+ \to Y$, and then $\Phi_0 = \Phi(\cdot, 1)$. The map ν is scale-invariant and surjective, and its fibres are the orbits of (7).*

(ii) A feature Ψ that does not use the scale is scale-invariant if and only if $\Psi = \Psi_0 \circ \pi_{\mathbf{q}}$ for a map $\Psi_0 : S_{\mathbf{q}} \to Y$, and then $\Psi_0 = \Psi|_{S_{\mathbf{q}}}$.

(iii) $\pi_{\mathbf{q}} \circ \nu(f, s) = \pi_{\mathbf{q}}(f)$ and $\rho_{\mathbf{q}}(\nu(f, s)) = s^{1/2} \rho_{\mathbf{q}}(f)$, and $(f, s) \mapsto \big(\pi_{\mathbf{q}}(f), s^{1/2} \rho_{\mathbf{q}}(f)\big)$ maps the orbit space of $(V^+ \smallsetminus 0) \times (0, \infty)$ bijectively onto $S_{\mathbf{q}} \times (0, \infty)$.

(iv) For all weights $\boldsymbol{\theta}$, $\nu_{\boldsymbol{\theta}}(\lambda \cdot (f, s)) = \lambda^{\boldsymbol{\theta}-\mathbf{q}} \star \nu_{\boldsymbol{\theta}}(f, s)$, where $\lambda^{\boldsymbol{\theta}-\mathbf{q}}\star$ multiplies V_k by $\lambda^{\theta_k - k}$. Hence $\nu_{\boldsymbol{\theta}}$ is scale-invariant if and only if $\boldsymbol{\theta} = \mathbf{q}$, and $\Phi_0 \circ \nu_{\boldsymbol{\theta}}$ is scale-invariant if and only if Φ_0 is constant on the orbits of the one-parameter group $\{\lambda^{\boldsymbol{\theta}-\mathbf{q}}\star\}_{\lambda>0}$, which is nontrivial for $\boldsymbol{\theta} \neq \mathbf{q}$.

(v) The retraction $\pi_{\boldsymbol{\theta}}$ is scale-invariant if and only if $\boldsymbol{\theta} = c\mathbf{q}$ for some $c > 0$. For $N \geq 2$ and every other $\boldsymbol{\theta}$, $\Psi_0 \circ \pi_{\boldsymbol{\theta}}$ is scale-invariant if and only if Ψ_0 is constant along the curves $\lambda \mapsto \pi_{\boldsymbol{\theta}}(\lambda \star u)$, $u \in S_{\boldsymbol{\theta}}$, which are not all constant; in particular Ψ_0 is not injective.

Proof. (i) $\nu(\lambda \cdot (f, s)) = (\lambda^2 s)^{1/2} \star \lambda^{-1} \star f = s^{1/2} \star f$, since $\star$ is an action, and $\nu(f, 1) = f$, so ν is surjective. If $\nu(f, s) = \nu(f', s')$, then $(f', s') = \lambda \cdot (f, s)$ with $\lambda = (s'/s)^{1/2}$, so the fibres of ν are the orbits. An invariant Φ therefore satisfies $\Phi(f, s) = \Phi\big(s^{-1/2} \cdot (f, s)\big) = \Phi(\nu(f, s), 1)$, and every $\Phi_0 \circ \nu$ is invariant. (ii) $\pi_{\mathbf{q}}$ is constant on the orbits of $\star$ and the identity on $S_{\mathbf{q}}$, and $f = \rho_{\mathbf{q}}(f) \star \pi_{\mathbf{q}}(f)$ (Thm. 2.2); so $\Psi(f) = \Psi(\pi_{\mathbf{q}}(f))$ for an invariant Ψ, and the converse is clear. (iii) The two identities are those of Thm. 2.2 with $\mu = s^{1/2}$. The map is invariant by (i), and its value (u, r) determines $\nu(f, s) = (s^{1/2} \rho_{\mathbf{q}}(f)) \star \pi_{\mathbf{q}}(f) = r \star u$, hence the orbit; every (u, r) is attained at $(r \star u, 1)$. (iv) $(\lambda^2 s)^{\theta_k/2} \lambda^{-k} = \lambda^{\theta_k - k} s^{\theta_k/2}$; the rest follows as in (i), since $\nu_{\boldsymbol{\theta}}(\cdot, 1)$ is the identity. (v) The fibres of $\pi_{\boldsymbol{\theta}}$ are the orbits of $\star_{\boldsymbol{\theta}}$, so $\pi_{\boldsymbol{\theta}}$ is scale-invariant if and only if for all λ and f there is $\mu > 0$ with $\lambda \star f = \mu \star_{\boldsymbol{\theta}} f$. For $\boldsymbol{\theta} = c\mathbf{q}$ take $\mu = \lambda^{1/c}$. Conversely, for f with all blocks nonzero, $\lambda f_1 = \mu^{\theta_1} f_1$ and $\lambda^k f_k = \mu^{\theta_k} f_k$ give $\mu = \lambda^{1/\theta_1}$ and $\theta_k = k\theta_1$ for every k. Since the actions $\star$ and $\star_{\boldsymbol{\theta}}$ commute and $f = \rho_{\boldsymbol{\theta}}(f) \star_{\boldsymbol{\theta}} \pi_{\boldsymbol{\theta}}(f)$, one has $\pi_{\boldsymbol{\theta}}(\lambda \star f) = \pi_{\boldsymbol{\theta}}(\lambda \star \pi_{\boldsymbol{\theta}}(f))$, which gives the last statement; for $\boldsymbol{\theta}$ not proportional to $\mathbf{q}$ and u with all blocks nonzero the curve is not constant, by the computation just made. □

Thm. 4.1 contains Theorem B.

Corollary 4.2. *A scale-invariant local feature factors through the normalized jet $\tilde{f} = s^{1/2} \star f$, and a scale-invariant feature that does not use the scale factors through $\pi_{\mathbf{q}}$; both maps are determined by the grades $\mathbf{q}$ of the jet. If a feature applies to the raw jet a normalization with weights $\boldsymbol{\theta} \neq \mathbf{q}$, or a retraction with weights $\boldsymbol{\theta}$ not proportional to $\mathbf{q}$, and is scale-invariant, then the layers that follow are constant along the orbits of a nontrivial one-parameter group, and the feature factors through $\tilde{f}$, or through $\pi_{\mathbf{q}}$, nonetheless.*

Proof. Parts (i) and (ii) of Thm. 4.1 give the first sentence, parts (iv) and (v) the second, and (i) and (ii) again the last clause. □

Case (i) is the scale normalization on which the Gaussian derivative networks [9] are built, and case (ii) is the graded retraction, which needs no scale. A normalization of the raw jet with equal grades, or with grades not proportional to $\mathbf{q}$, is excluded by (iv) and (v). The theorem does not require the weights $\mathbf{q}$ in the first normalization of a network: since $\pi_{\mathbf{q}}(\nu_{\gamma\mathbf{q}}(f, s)) = \pi_{\mathbf{q}}(f)$ for every $\gamma > 0$, an invariant feature may follow a γ-normalization that is not itself invariant, and by Thm. 4.2 it then factors through $\pi_{\mathbf{q}}$. The two factorizations differ in content: the bundle quotient keeps the invariant $s^{1/2}\rho_{\mathbf{q}}(f)$ of part (iii), which the fibre quotient discards, and which the networks of Sec. 6 use only in a foreground gate. Under blur the two realizations behave differently.

5. Blur and the scale direction

5.1. **Unknown blur.** An image may arrive already smoothed: by defocus, by a reduction of resolution, or by optics whose blur is fixed in pixels while the object is seen smaller. We model this by $I' = g_b * I$ with an unknown $b > 0$. Since $g_s * g_b = g_{s+b}$, the jet of I' at the scale s is the jet of I at the scale $s + b$. For an image $I \geq 0$ of finite positive mass and finite second moment, let $\bar{x}_I$ and $\hat{\sigma}_I$ be the mean and the root-mean-square radius of the probability density $I/\int I$, so that $\hat{\sigma}_I^2 = \int |x - \bar{x}_I|^2 I(x)\, dx/\int I$; we call $(\bar{x}_I, \hat{\sigma}_I)$ the *intensity frame* of I.

Proposition 5.1. *Let $b > 0$, $I' = g_b * I$, $\mu = \big(s/(s+b)\big)^{1/2} \in (0, 1)$, and let $u = \nu\big(f^I(x; s+b), s+b\big)$ be the normalized jet of I at the scale $s + b$. For every x, every $s > 0$ and every $c > 0$:*

(i) $f^{cI'}(x; s) = c\, f^I(x; s+b)$, and for $J = c\,(g_b * D_\lambda I)$, $f^J(\lambda x; s) = c\,\lambda^{-1} \star f^I\big(x; (s+b)/\lambda^2\big)$;

(ii) $\pi_{\mathbf{q}}\big(f^{I'}(x; s)\big) = \pi_{\mathbf{q}}\big(f^I(x; s+b)\big)$, whereas $\nu\big(f^{I'}(x; s), s\big) = \mu \star u$, and $\pi_{\mathbf{1}}(\mu \star u) \neq \pi_{\mathbf{1}}(u)$ unless all nonzero blocks of u have the same order;

(iii) $\pi_{\mathbf{q}}\big(f^{cI'}(x; s)\big) = \pi_{\mathbf{q}}(c\,u)$ and $\pi_{\mathbf{1}}\big(\nu(f^{cI'}(x; s), s)\big) = \pi_{\mathbf{1}}(\mu \star u)$;

(iv) $s^{1/2}\rho_{\mathbf{q}}\big(f^{cI'}(x; s)\big) = \mu\, \rho_{\mathbf{q}}(c\,u)$ and $\|\nu(f^{cI'}(x; s), s)\| = c\big(\sum_k \mu^{2k}\|u_k\|^2\big)^{1/2}$;

(v) if $I \geq 0$ has finite positive mass and finite second moment, then $\bar{x}_J = \lambda \bar{x}_I$ and $\hat{\sigma}_J^2 = \lambda^2 \hat{\sigma}_I^2 + 2b$.

In (ii)–(iv) the same holds for J, with $(s+b)/\lambda^2$ in place of $s + b$ and the same μ.

Proof. (i) $g_s * g_b = g_{s+b}$, linearity, and Thm. 2.1. (ii) and (iii) $s^{1/2} \star f = \mu \star \big((s+b)^{1/2} \star f\big)$, since $\star$ is an action and commutes with scalar multiplication; $\pi_{\mathbf{q}}$ is constant on the orbits of $\star$ (Thm. 2.2) and $\pi_{\mathbf{1}}$ on the rays $u \mapsto cu$. If $\pi_{\mathbf{1}}(\mu \star u) = \pi_{\mathbf{1}}(u)$ with $\mu \neq 1$, then $\mu^k u_k = a\, u_k$ for one $a > 0$ and every nonzero block, which forces the orders of the nonzero blocks to coincide. (iv) The homogeneity of $\rho_{\mathbf{q}}$ under $\star$, and the definition of the Euclidean norm. (v) Normalize the intensity to a probability density. Convolution with g_b adds an independent centred Gaussian vector of covariance $b\,\mathrm{Id}$, which keeps the mean and adds its trace $2b$ to the squared radius; a dilation multiplies the mean by λ and the squared radius by λ^2, and c does not change the density. For J, apply (i) and Thm. 2.1: $s^{1/2} \star \lambda^{-1} \star f = \mu \star \big((s+b)/\lambda^2\big)^{1/2} \star f$. □

Thm. 5.1(i) and (ii) prove Theorem C. Blur acts on the retracted jet and on the normalized jet alike by the change of scale $s \mapsto s + b$, and on the normalized jet in addition by the grading factor $\mu\star$, with $\mu^2 = s/(s+b)$ smallest at the finest scales. Without a contrast factor the retracted jet of the blurred image is that of the sharp image at a coarser scale, of the kind a network evaluated on a ladder of scales encounters in training. The radial projection does not remove the grading factor, and at fine

scales the normalized jet of the blurred image moves to jets that sharp images do not produce. By (iii), a contrast factor behaves the other way: the retraction keeps it and the radial projection removes it. Normalizing by $s+b$ in place of s would correct the scale normalization, but only for a known b; the retraction needs neither s nor b. Lindeberg's networks normalize the derivatives of each layer by the nominal scale of that layer, so (ii) applies to their first layer, while their later layers smooth further, at scales that grow with depth.

Thm. 5.1 concerns features and is not an invariance statement. First, the retraction is not invariant under blur at a fixed position and scale: for $I(x) = e^{-|x|^2/2}$ and $x_s = (\sqrt{1+s}, 0)$, the second derivative of $g_s * I$ in x_1 vanishes at x_s while the first does not, and after a blur of variance b it equals $-b(1+s+b)^{-3}\exp\big(-\frac{1+s}{2(1+s+b)}\big) \neq 0$. The grading action multiplies the whole second block by one positive factor and cannot make a vanishing coordinate nonzero, so $\pi_{\mathbf{q}}\big(f^{I'}(x_s;s)\big) \neq \pi_{\mathbf{q}}\big(f^{I}(x_s;s)\big)$. Second, $s \mapsto s+b$ is an additive change, not a shift of a geometric ladder of scales, and by (iv) and (v) the scale-normalized energies and the intensity frame change as well, so a feature pooled over positions and scales need not be preserved. Third, a contrast normalization after the blur introduces a factor $c_b = 1/\sup(g_b * I)$, which by (iii) the retraction keeps. How the robustness of the features carries over to predictions is measured in Sec. 8.3.

5.2. **Between scales.**

Lemma 5.2. *Let $\Delta : V_{k+2} \to V_k$ be the contraction $\Delta_k = \frac{1}{(k+1)(k+2)}(\partial_\xi^2 + \partial_\eta^2)$, acting componentwise on sequences $(f_k)_{k\geq 0}$ of forms, and let E be the grading operator, $Ef_k = kf_k$. Let I be a bounded measurable image and $f = (f_k)_{k\geq 0}$ the full jet of $L(\cdot;s) = g_s * I$.*

(i) $\partial_s f_k = \frac{1}{2}\,\Delta_k\, f_{k+2}$ for $s > 0$, and $[E, \Delta] = -2\,\Delta$.

(ii) For $0 < s' < 2s$ and $\mu = (s'/s)^{1/2}$ the series

$$\tilde{f}_k(x;s') = \mu^k \sum_{j\geq 0} \frac{1}{j!}\Big(\frac{\mu^2-1}{2}\Big)^j\, \Delta^j\, \tilde{f}_{k+2j}(x;s)$$

converges for every k; we write it as

$$\tilde{f}(x;s') = \mu \star \exp\Big(\tfrac{\mu^2-1}{2}\,\Delta\Big)\tilde{f}(x;s). \tag{8}$$

If I is a polynomial, the sums are finite and (8) holds for every $s' > 0$.

Proof. (i) With (1) and the heat equation $\partial_s L = \frac{1}{2}(L_{xx} + L_{yy})$, the coefficient of $\binom{k}{a}\xi^a\eta^b$ in $\partial_s f_k$ is $\frac{1}{2}(L_{(a+2,b)} + L_{(a,b+2)})$, and $\frac{1}{(k+1)(k+2)}(\partial_\xi^2 + \partial_\eta^2)$ applied to (1) with $k+2$ in place of k gives $\sum_{a+b=k}\binom{k}{a}(L_{(a+2,b)} + L_{(a,b+2)})\xi^a\eta^b$, as the identity $\binom{k+2}{a+2}(a+2)(a+1) = (k+2)(k+1)\binom{k}{a}$ shows. Since Δ lowers the degree by two, $E\,\Delta\, v = (k-2)\,\Delta\, v = \Delta\, Ev - 2\,\Delta\, v$. (ii) By (i), $\partial_s^j f_k = 2^{-j}\,\Delta^j\, f_{k+2j}$. For $\operatorname{Re} z > 0$ the kernel $g_z(x) = (2\pi z)^{-1}\exp(-|x|^2/2z)$ and its derivatives are integrable, so for bounded I the function $z \mapsto (\partial^\alpha g_z * I)(x)$ is holomorphic on $\operatorname{Re} z > 0$, and its Taylor series at s converges to it on the disc $|z-s| < s$. For $0 < s' < 2s$ this gives $f_k(s') = \sum_j \frac{(s'-s)^j}{2^j j!}\,\Delta^j\, f_{k+2j}(s)$, and then

$$\tilde{f}_k(s') = s'^{k/2}\sum_j \frac{(s'-s)^j}{2^j j!}\,\Delta^j\, f_{k+2j}(s) = \Big(\frac{s'}{s}\Big)^{k/2}\sum_j \frac{1}{j!}\Big(\frac{s'-s}{2s}\Big)^j\,\Delta^j\big(s^{(k+2j)/2} f_{k+2j}(s)\big),$$

which is (ii) with $(s'-s)/s = \mu^2 - 1$. For a polynomial image $L(x;s)$ is a polynomial in s and $\Delta^j\, f_{k+2j} = 0$ for large j. □

The component of order k at s' involves all the orders $k+2j$ at s, so the N-jet at s' is not a function of the N-jet at s. In (8) the factor $\mu\star$ is the grading action, and the factor $\exp(\frac{\mu^2-1}{2}\,\Delta)$ is triangular with respect to the derivative order, with the identity on the diagonal: it adds to each order a combination of the orders above it. On the finite jets of polynomial images it is unipotent; on the full jet of a general image the series in Δ does not terminate. Beyond $s' = 2s$ the series need not converge:

for $I(x) = e^{-|x|^2/2a}$ one has $L(0;s) = a/(a+s)$, whose Taylor series at s has radius $s+a$ and diverges for $s' > 2s+a$, arbitrarily close to $2s$ as $a \to 0$.

Let the jet be computed on a geometric ladder of scales $s_i = s_0\kappa^i$ with $1 < \kappa \leq 2$, as in the networks of Sec. 6. Under a dilation by a factor λ that is not a power of $\kappa^{1/2}$, the jet of $D_\lambda I$ at $(\lambda x; s_j)$ is, by Thm. 2.1, $\lambda^{-1} \star f^I(x; s_j/\lambda^2)$, the jet of I at a scale strictly between two rungs. Comparing it with the jet of I at the rung s_i below is the situation of Thm. 5.2 with $s = s_i$ and $s' = s_j/\lambda^2 < 2s_i$.

Proposition 5.3. *Let $0 < s' < 2s$, $\mu = (s'/s)^{1/2}$, and let*

$$R_k(s) = \sum_{j \geq 1} \frac{1}{j!} \left(\frac{\mu^2 - 1}{2}\right)^j \Delta^j \, \tilde{f}_{k+2j}(s)$$

be the heat correction of Thm. 5.2. For the jets of positive order at most N, whenever the jets involved are nonzero,

$$\pi_{\mathbf{q}}(\tilde{f}(s')) = \pi_{\mathbf{q}}(\tilde{f}(s) + R(s)), \qquad \pi_{\mathbf{1}}(\tilde{f}(s')) = \pi_{\mathbf{1}}(\mu \star (\tilde{f}(s) + R(s))).$$

Let $h = (\tilde{f}_k(s))_{k=1}^N$, $a = (\Delta_k \, \tilde{f}_{k+2}(s))_{k=1}^N$, $\delta = \mu^2 - 1$ and $(Eh)_k = kh_k$. If every block of h is nonzero, then, as $\delta \to 0$,

$$\pi_{\mathbf{q}}(\tilde{f}(s')) = \pi_{\mathbf{q}}(h) + \tfrac{\delta}{2} \, d\pi_{\mathbf{q}}(h)[a] + O(\delta^2),$$
$$\pi_{\mathbf{1}}(\tilde{f}(s')) = \pi_{\mathbf{1}}(h) + \tfrac{\delta}{2} \, d\pi_{\mathbf{1}}(h)[Eh + a] + O(\delta^2).$$

Proof. The identities follow from Thm. 5.2 and Thm. 2.2. The convergent heat expansion gives $h + \delta a/2 + O(\delta^2)$ once the grading factor is removed. Since $\mu^k = (1+\delta)^{k/2} = 1 + k\delta/2 + O(\delta^2)$, keeping that factor gives $h + \delta(Eh + a)/2 + O(\delta^2)$. The two retractions are smooth at a point with nonzero blocks (Thm. 2.3), and a Taylor expansion proves the formulas. The constants depend on the image, the position and the scale. □

To first order the retraction removes the grading term Eh and keeps only the heat correction a, while the radial projection keeps both. The formulas do not by themselves order the sizes of the two residuals. The radial projection quotients the normalized jet by scalar multiplication, which is the contrast factor of Sec. 2.4, and the retraction quotients it by the grading action; quotienting by both, that is by the torus T, would remove one more dimension (Thm. 2.4). Between two scales the normalized jet changes by the grading factor and the heat correction, not by a scalar factor (Thm. 5.2); with contrast removed at the input, the scalar factor that a radial normalization removes is the local intensity of the image, not an effect of the zoom. Which realization is closer between rungs depends on the size of the heat correction. For digit strokes, whose width is comparable to the finer rungs, it is not negligible (Sec. A.2), so between rungs neither realization has a guaranteed advantage.

6. Graded networks

6.1. **Layers.** Fix an order N, grades $\boldsymbol{\theta}$ and a geometric ladder of scales $s_i = s_0\kappa^i$, $i = 0, \ldots, n-1$, with $\kappa > 1$. A *graded network with grades $\boldsymbol{\theta}$* computes, at every position x of a sampling grid and every scale s_i, the jet $f(x; s_i)$ of (1), retracts it to $\pi_{\boldsymbol{\theta}}(f(x; s_i))$, and applies to the retracted jet a pointwise map that is equivariant under rotations. The weights are shared across positions and scales.

The pointwise map acts on complex *slots*. A slot has a type (w, j), where w is a formal weight, the total derivative order, and $j \geq 0$ is a frequency; a rotation by ϕ multiplies a slot of frequency j by $e^{ij\phi}$, and each type carries m channels. The harmonic coordinates $c_{k,j}$ of the retracted jet are the input slots, of types (k, j). There are three kinds of layers.

(a) *Complex-linear maps*, applied type by type with the same weights at every position and scale. For $j \geq 1$ they are, by Schur's lemma, the general SO(2)-equivariant real-linear maps between slots of frequency j; for $j = 0$, where SO(2) acts trivially, they form a proper subset of the real-linear maps, which suffices for what follows. As convolutions with a 1×1 kernel and grade shift zero they commute with translations and, by Thm. 3.2, with dilations; they are the graded linear maps of degree zero of [1].

(b) *Products*. For slots z of type (w, j) and z' of type (w', j') the products zz' and $z\bar{z}'$ have the types $(w + w', j + j')$ and $(w + w', |j - j'|)$, the conjugate being stored when $j < j'$. In the harmonic basis their complex multiples are the SO(2)-equivariant bilinear maps into slots of positive frequency, and the real and imaginary parts of the products of frequency zero span, over $\mathbb{R}$, the invariant bilinear forms. They realize the graded tensor products of [1] compatibly with rotations, and the transvectants of classical invariant theory, which are the SL_2-equivariant bilinear maps on binary forms [13], are linear combinations of them; for instance $(f_2, f_2)^{(2)} = 2 \det \mathrm{Hess}\, L$. A product layer forms the channelwise products of its input slots with the input jet slots for all pairs of types with $w + w' \le w_{\max}$, appends its input slots, and maps each type to m channels by a layer of kind (a).

(c) *Gates* $z \mapsto \sigma(\alpha(|z| - \beta))\, z$, with σ the logistic function, α fixed and β learnable per channel; they are equivariant because $|z|$ is invariant.

After the retraction every slot is invariant under the grading action, so the gates need no normalization, and no other nonlinearity is used. The slots of the last layer are read as real numbers. The *full readout* takes the real and imaginary parts of every slot, which transform under rotations and keep the orientation; the *invariant readout* takes $|z|$ for every slot and the real and imaginary parts of the slots of frequency zero. A learnable linear map reduces them to a position feature $\psi(x, s_i) \in \mathbb{R}^{m'}$.

6.2. **Pooling in the image frame.** Let $(\bar{x}, \hat{\sigma})$ be the intensity frame (Sec. 5.1) of the contrast-normalized image. A position x at the scale s has the coordinates

$$r = |x - \bar{x}|/\hat{\sigma}, \qquad \tau = \log(\sqrt{s}/\hat{\sigma}),$$

which are invariant under translations and under a dilation D_λ combined with $s \mapsto \lambda^2 s$. The pooling uses finitely many bins $b = 1, \dots, B$ with centres (c_b^r, c_b^τ), widths (ω_r, ω_τ) and the memberships

$$m_b(x, s) = \tfrac{1}{2}\big(1 + \cos(\pi d_b/2)\big) \ \text{ if } d_b < 2, \qquad m_b(x, s) = 0 \ \text{ otherwise}, \qquad d_b^2 = \frac{(r - c_b^r)^2}{\omega_r^2} + \frac{(\tau - c_b^\tau)^2}{\omega_\tau^2}.$$

A foreground gate $g = \sigma\big(a_0(\log \tilde{\rho} - b_0)\big)$, with a_0 and b_0 learnable and $\tilde{\rho}$ a scale-normalized energy of the jet, and the area $A(s)$ of the sampling cell at the scale s give the weights $w(x, s) = g(x, s)\, A(s)/s$. The pooled vector consists of the weighted means and the relative masses

$$\Phi_b = \frac{\sum_{x,s} w\, m_b\, \psi}{\sum_{x,s} w\, m_b}, \qquad M_b = \frac{\sum_{x,s} w\, m_b}{\sum_{b'} \sum_{x,s} w\, m_{b'}},$$

and a layer normalization followed by a two-layer perceptron maps it to the output. The grades enter in two places only, the retraction and the foreground gate. A plain average over positions and scales would not be invariant: it is dominated by the finest rungs, which have the most positions, and a shift of the ladder changes which rungs are present. The pooling weights every rung by its area per unit scale and places it by its scale relative to the image.

6.3. **Three networks.**

Definition 6.1. The *graded convolutional network* GCN is the graded network with $\boldsymbol{\theta} = \mathbf{q}$ and foreground energy $\tilde{\rho} = \rho_{\mathbf{q}}(\tilde{f}) = s^{1/2} \rho_{\mathbf{q}}(f)$.

Definition 6.2. The *equal-grades twin* UCN is GCN with $\boldsymbol{\theta} = (1, \dots, 1)$: the same jet layer on the same ladder and the same layers, pooling and perceptron, with $\rho_{\boldsymbol{\theta}}$ the Euclidean norm, $\pi_{\boldsymbol{\theta}} = \pi_{\mathbf{1}}$ the radial projection and $\tilde{\rho} = s^{1/2} \|f\|$.

Definition 6.3. The *scale-normalized twin* SNT is UCN applied to the normalized jet, with $\pi_{\mathbf{1}}(\tilde{f})$ in place of $\pi_{\mathbf{1}}(f)$ and $\tilde{\rho} = \|\tilde{f}\|$.

In the experiments $N = 3$ and the ladder is $s_i = 2^{i+1}$, $i = 0, \dots, 11$, in pixels of the working grid (Sec. A.1). The lift has $m = 8$ channels per type and is followed by a gate; one product layer with $w_{\max} = 6$, which has 15 slot types and 120 slots, is followed by a gate; the full readout is reduced to $m' = 16$; the 3×3 bins have the centres $c^r \in \{0.5, 1, 1.5\}$ and $c^\tau \in \{-1, -0.5, 0\}$ and the widths

$\omega_r = \omega_\tau = 0.3$; and the perceptron has 64 hidden units. Each of the three networks has 21,950 parameters: 7,280 in the equivariant layers, 3,856 in the reduction, 10,506 in the perceptron and 308 in the layer normalization and the foreground gate.

By Thm. 4.1, GCN is invariant under the grading action at a fixed scale, SNT under dilations at corresponding scales, and UCN under neither, only under the scalar multiplication $f \mapsto cf$, which is contrast. A dilation by $\kappa^{1/2}$ acts by a shift of the ladder index (Thm. 2.1), so a network on $\tilde{f}$, or on $\pi_{\mathbf{q}}(f) = \pi_{\mathbf{q}}(\tilde{f})$, with weights shared across the ladder is equivariant under the discrete group generated by $\kappa^{1/2}$, up to the ends of the ladder. The scale-equivariant networks of [19, 20] carry such a ladder as well; the continuous group within one rung is described by Thms. 5.2 and 5.3.

6.4. **Invariance.**

Lemma 6.4. *The coordinates r and τ and the memberships m_b are invariant under translations and under the dilation D_λ composed with the ladder shift $s \mapsto \lambda^2 s$. So are the foreground gates of* GCN *and* SNT*, which are functions of $\tilde{f}$ (Thm. 4.1), and so is w when λ is a power of two, for which the dilation maps the sampling pyramid of a canvas onto that of the dilated canvas, with the rung index shifted (Sec. A.1). Hence the pooled vectors of* GCN *and* SNT *are invariant under the dilations by powers of two, provided the bins are supported inside the ladder. In the continuous idealization, in which the sums over the pyramid are integrals over all positions and scales, they are invariant under all translations. Under the rotations by multiples of $90°$, which preserve the sampling grid, the bins are invariant, the slots transform by their frequencies, and the pooled vector of the invariant readout is invariant.*

The full readout, followed by an unconstrained reduction and perceptron, carries no guarantee under rotations; it keeps the orientation. The bins are supported inside the ladder for all images whose radius $\hat{\sigma}$ keeps $c_b^\tau \pm 2\omega_\tau$ within $[\log(\sqrt{s_0}/\hat{\sigma}), \log(\sqrt{s_{n-1}}/\hat{\sigma})]$. Outside this range of sizes a bin is partly empty and the invariance holds only approximately, as for every network on a finite ladder of scales.

Proposition 6.5. *Let $\boldsymbol{\theta}$ be a grading and $\Phi_{\boldsymbol{\theta}}$ the position features of Sec. 6.1 built on $\pi_{\boldsymbol{\theta}}$.*

- *(i) $\Phi_{\boldsymbol{\theta}}(\mu \star_{\boldsymbol{\theta}} f) = \Phi_{\boldsymbol{\theta}}(f)$ for all $\mu > 0$; in particular $\Phi_{\mathbf{q}}$ is invariant under the dilation action on the jet at a fixed scale, and $\Phi_{(1,\dots,1)}$ is invariant under $f \mapsto cf$, whereas $\pi_{(1,\dots,1)}$ is not constant on the orbits of $\star_{\mathbf{q}}$.*
- *(ii) Every slot of frequency j is multiplied by $e^{ij\phi}$ under the rotation by ϕ, and the invariant readout is rotation-invariant.*
- *(iii) On the ladder, $\Phi_{\mathbf{q}}$ evaluated on $D_\lambda I$ at (x, s) equals $\Phi_{\mathbf{q}}$ evaluated on I at $(x/\lambda, s/\lambda^2)$ for every λ; for $\lambda = \kappa^{m/2}$ this is a shift of the ladder index by m. The same holds for the position features of* SNT*, which are functions of $\tilde{f}$. The pooled vectors of* GCN *and* SNT *are invariant under the dilations by powers of two and, in the continuous idealization, under translations, with the provisos of Thm. 6.4.*

Proof. (i) is Thm. 2.2 together with the fact that every later layer is a function of $\pi_{\boldsymbol{\theta}}(f)$; the last assertion holds because the radial projection of $\mu \star_{\mathbf{q}} f$ differs from that of f unless all nonzero components of f have the same order (Thm. 5.1(ii)). (ii) is (4) together with the rule for products. (iii) is Thm. 2.1 with $\pi_{\mathbf{q}}(\tilde{f}) = \pi_{\mathbf{q}}(f)$, Thm. 4.1(i) for SNT, and Thm. 6.4. □

6.5. **Universality.**

Theorem 6.6. *Let $F : V^+ \smallsetminus 0 \to \mathbb{R}$ be continuous and invariant under dilations and rotations, and let $K \subset V^+ \smallsetminus 0$ be compact. For every $\varepsilon > 0$ there is a pointwise graded network $\widehat{F}$ with invariant readout and enough product layers, channels, weight cutoff $w_{\max}$ and perceptron width, such that $\sup_K |F - \widehat{F}| < \varepsilon$.*

Proof. We apply the invariant-polynomial construction of [27] after the weighted retraction. Write $F = F_0 \circ \pi_{\mathbf{q}}$ with F_0 continuous and SO(2)-invariant on the compact weighted sphere $S_{\mathbf{q}}$; this is possible since $\pi_{\mathbf{q}}$ is continuous and constant on the dilation orbits. In the harmonic coordinates

$c = (c_{k,j})$ the circle acts by (4), a torus action with integer weights, and $\mathbb{R}[V^+]^{\mathrm{SO}(2)}$ is generated by the real and imaginary parts of the finitely many minimal monomials $\prod c_{k,j}^{a_{k,j}} \bar{c}_{k,j}^{b_{k,j}}$ of total frequency $\sum j(a_{k,j} - b_{k,j}) = 0$, by Gordan's lemma on the semigroup of exponents [15]. The invariants of a compact group separate its orbits, which are closed [14, 15]. Let $p = (p_1, \dots, p_r)$ be the generators. The map $p : S_{\mathbf{q}}/\mathrm{SO}(2) \to \mathbb{R}^r$ is a continuous injection of a compact space into a Hausdorff space, hence a homeomorphism onto its image Q, so $F_0 = F_1 \circ p$ with F_1 continuous on Q. Extend F_1 to $\mathbb{R}^r$ by Tietze's theorem and approximate it uniformly on a ball by a perceptron with one ReLU hidden layer [16, 32]. It remains to approximate p uniformly on $S_{\mathbf{q}}$. A monomial $\prod c_{k,j}^{a_{k,j}} \bar{c}_{k,j}^{b_{k,j}}$ of degree d is a product of d jet slots, of weight $\sum_{k,j} k(a_{k,j} + b_{k,j})$, which lies between d and Nd. If $w_{\max}$ is at least the largest weight of the generators, the product layer keeps every partial product, and $d - 1$ product layers form the monomial when the gates are replaced by the identity and the layers of kind (a) select channels; the invariant readout returns its real and imaginary parts as slots of frequency zero. A gate $z \mapsto \sigma(\alpha(|z| - \beta))z$ converges to the identity uniformly on bounded sets as $\beta \to -\infty$, and all slots are bounded on the compact set $S_{\mathbf{q}}$, so the network with its gates approximates p uniformly on $S_{\mathbf{q}}$. Since F_1 is uniformly continuous on a compact neighbourhood of Q, the composite approximates $F_0 \circ \pi_{\mathbf{q}}$ uniformly on K. □

6.6. **Pointwise predictors along scale orbits.** The next two results concern pointwise predictors on a single jet; the separation for complete classifiers, with foreground gates and pooling, is Thm. 7.2. Write $x = \mu \star \tilde{x}$ with $\tilde{x} = \pi_{\mathbf{q}}(x) \in S_{\mathbf{q}}$ and $\mu = \rho_{\mathbf{q}}(x)$ for the orbit coordinates of a jet.

Theorem 6.7. *Let x be a random jet in $V^+ \smallsetminus 0$ and $y = F(x) + \epsilon$, where F is dilation-invariant with $\mathbb{E}F(x)^2 < \infty$ and ϵ is independent of x with mean zero and $\mathbb{E}\epsilon^2 < \infty$, and let $\mathrm{R}(\widehat{f}) = \mathbb{E}(\widehat{f}(x) - y)^2$. For every square-integrable predictor $\widehat{f}$ the orbit average $\bar{f}(x) = \mathbb{E}[\widehat{f}(x) \mid \pi_{\mathbf{q}}(x)]$ is dilation-invariant and*

$$\mathrm{R}(\widehat{f}) - \mathrm{R}(\bar{f}) = \mathbb{E}\ \mathrm{Var}\big(\widehat{f}(x) \mid \pi_{\mathbf{q}}(x)\big)\ \geq 0,$$

with equality if and only if $\widehat{f}(x)$ is almost surely a function of $\pi_{\mathbf{q}}(x)$. In particular $\mathrm{R}(\widehat{f}) - \mathrm{R}(F) \geq \mathbb{E}\ \mathrm{Var}\big(\widehat{f}(x) \mid \pi_{\mathbf{q}}(x)\big)$.

Proof. Condition on $\tilde{x} = \pi_{\mathbf{q}}(x)$. Since $F(x) = F_0(\tilde{x})$ and ϵ is independent,

$$\mathbb{E}\big[(\widehat{f}(x) - y)^2 \mid \tilde{x}\big] = \mathrm{Var}(\widehat{f} \mid \tilde{x}) + \big(\mathbb{E}[\widehat{f} \mid \tilde{x}] - F_0(\tilde{x})\big)^2 + \mathbb{E}\epsilon^2,$$

and the last two terms are the conditional risk of $\bar{f}$. Taking expectations gives the identity; no assumption on the law of μ given $\tilde{x}$ is needed, so no Haar measure on the noncompact group is required. The last inequality follows from $\mathrm{R}(\bar{f}) \geq \mathrm{R}(F)$, since $F(x) = \mathbb{E}[y \mid x]$. □

A pointwise graded predictor after retraction has orbit variance zero by Thm. 6.5(i). The orbit average $\bar{f}$ is only measurable, but it is an L^2 limit of continuous dilation-invariant functions, since continuous functions are dense in L^2 of the law of $\pi_{\mathbf{q}}(x)$ on the compact space $S_{\mathbf{q}}$, and those of them that are also rotation-invariant are approximated by graded networks by Thm. 6.6.

Theorem 6.8. *Consider pointwise predictors on a single jet, after the retraction and before the foreground gate and the pooling. Fix $\tilde{x} \in S_{\mathbf{q}}$ with $\tilde{x}_N \neq 0$ and consider the orbit $\mu \mapsto \mu \star \tilde{x}$.*

- *(i) If $\widehat{f}$ is a network on V with affine layers and activations with finitely many affine pieces, such as a ReLU perceptron or a ReLU convolutional network read through the jet, then $\mu \mapsto \widehat{f}(\mu \star \tilde{x})$ coincides for all sufficiently large μ with a polynomial of degree at most N in μ; unless that polynomial is constant, $|\widehat{f}(\mu \star \tilde{x})| \to \infty$.*
- *(ii) If $\widehat{f}$ is a pointwise* UCN, *then $\lim_{\mu \to \infty} \widehat{f}(\mu \star \tilde{x})$ exists and depends only on $\tilde{x}_N / \|\tilde{x}_N\|$, with convergence at the rate μ^{-1}, and $\lim_{\mu \to 0} \widehat{f}(\mu \star \tilde{x})$ depends only on the lowest nonzero component of $\tilde{x}$.*
- *(iii) A pointwise* GCN *satisfies $\widehat{f}(\mu \star \tilde{x}) = \widehat{f}(\tilde{x})$ for all $\mu > 0$.*

Proof. (i) A network with affine layers and piecewise-linear activations is affine on each cell of a finite polyhedral partition of V. The curve $\mu \mapsto \mu \star \tilde{x} = (\mu^k \tilde{x}_k)_k$ is polynomial in μ, so each of the finitely many hyperplanes that bound the cells is crossed at finitely many μ or contains the curve. Beyond the largest crossing the curve stays in the closure of one cell, on which $\widehat{f}(\mu \star \tilde{x}) = c + \sum_k \mu^k \langle w_k, \tilde{x}_k \rangle$. (ii) The radial projection of $\mu \star \tilde{x}$ converges as $\mu \to \infty$ to $(0, \dots, 0, \tilde{x}_N / \|\tilde{x}_N\|)$ with error $O(\mu^{-1})$, and as $\mu \to 0$ to the unit vector along the lowest nonzero component. The rest of the pointwise network is Lipschitz on the compact sphere, since its linear maps, bounded products, gates and readout are Lipschitz there. (iii) is Thm. 6.5(i). □

At either end of a fibre orbit the pointwise UCN thus retains a single derivative order. The proof of Thm. 6.7 uses only that $\pi_{\mathbf{q}}$ is a complete invariant of the dilation action on the fibre. With the action (7) and its complete invariant ν (Thm. 4.1) in place of $\pi_{\mathbf{q}}$ the same identity holds, and GCN and SNT both have orbit variance zero for it. Thm. 6.8 concerns the action on the fibre at a fixed scale. There SNT is the radial projection of a fixed multiple of the jet and behaves like UCN; but a dilation of the image acts by (7), not on the fibre at a fixed scale, and for that action SNT is invariant. The variance along zooms of images measured in Sec. 8 vanishes for the ideal pooled graded network only under the matching and support conditions of Thms. 6.4 and 6.5, which sampled digits need not meet exactly.

7. Separation at the zero jet

By Thm. 2.3 the retraction $\pi_{\mathbf{q}}$ has no continuous extension to the zero jet. In this section we show that at this point the graded quotient separates families of images that every radial normalization, and every classifier continuous in the image, confuses. Throughout, $u_1 \in V_1$ has norm one and $u_2 \in V_2$ is the positive isotropic quadratic form of norm one, whose only nonzero harmonic coordinate is the trace coordinate h_0 of Sec. 2.2.

7.1. **Probe classifiers.** Fix finitely many distinct position–scale probes $\mathcal{P} = \{(x_p, s_p) : p = 1, \dots, P\}$ with $s_p > 0$ and finitely many bins $b = 1, \dots, B$, and write $\mathcal{J}_p I = (f_{1,p}, f_{2,p}, f_{3,p})$ for the exact Gaussian 3-jet of positive order of an image I at the probe p. Let π be one of the normalizations $\pi_{\mathbf{q}}$, the radial projection $\pi_{\mathbf{1}}(f) = f/\|f\|$ of the raw jet, or the radial projection $\pi_{\mathbf{1}} \circ \nu$ of the normalized jet, each extended by $\pi(0) = 0$.

Definition 7.1. A *probe classifier with normalization* π is a function $H(I) = \Omega\big(\Phi(I), M(I)\big)$ with

$$\Phi_b(I) = \frac{\sum_p w_p(I)\, m_{bp}(I)\, \psi\big(\pi(\mathcal{J}_p I)\big)}{\sum_p w_p(I)\, m_{bp}(I) + \eta}, \qquad M_b(I) = \frac{\sum_p w_p(I)\, m_{bp}(I)}{\sum_{b',p} w_p(I)\, m_{b'p}(I)},$$

where $\eta \geq 0$, empty means and masses are zero, and

- (P1) $\psi : \pi(V^+) \to \mathbb{R}^d$ is bounded and Lipschitz;
- (P2) the weights $w_p(I) \geq 0$ are functions of the block norms $\|f_{k,p'}\|$, the scales and the intensity frame and mass of I, and the memberships $m_{bp}(I) \in [0, 1]$ are fixed functions of the probe and the intensity frame;
- (P3) Ω is Lipschitz on bounded sets.

For given probes, bins and memberships, $\mathcal{N}_\pi$ denotes the class of probe classifiers with normalization π.

Weights that depend on block norms include foreground gates and hard thresholds on them. For images $I_t^{\pm}$ with labels ± 1 let

$$R_t(H) = \tfrac{1}{2}\big\{(H(I_t^+) - 1)^2 + (H(I_t^-) + 1)^2\big\}, \qquad C_t(H) = \tfrac{1}{2}\big\{\log(1 + e^{-H(I_t^+)}) + \log(1 + e^{H(I_t^-)})\big\}$$

be the balanced squared and logistic losses.

7.2. **The separation theorem.**

Theorem 7.2. *Let the probes contain $p_0 = (0, s_*)$, and let the memberships be those of the pooling of Sec. 6.2 with the bins of Sec. 6.3. There are $t_0 > 0$ and smooth compactly supported images $I_t^{\pm} : \mathbb{R}^2 \to [0,1]$, $0 < t < t_0$, with minimum 0 and maximum 1, such that:*

(i) *the intensity frames and masses of $I_t^{\pm}$ and their jets at the probes $p \neq p_0$ do not depend on t or on the sign, $\mathcal{J}_{p_0} I_t^{\pm} = (tu_1, \pm t^2 u_2, 0)$, the images converge uniformly to one image I_0 as $t \to 0$, and p_0 has positive membership in some bin;*

(ii) *for every $H \in \mathcal{N}_{\pi_{\mathbf{1}}}$ there is $K_H < \infty$ with*

$$|H(I_t^+) - H(I_t^-)| \le \frac{2K_H t}{\sqrt{1+t^2}}, \qquad R_t(H) \ge \Big(1 - \frac{K_H t}{\sqrt{1+t^2}}\Big)_+^2, \qquad C_t(H) \ge \log\Big(1 + e^{-K_H t/\sqrt{1+t^2}}\Big),$$

and the same holds for every $H \in \mathcal{N}_{\pi_{\mathbf{1}} \circ \nu}$ with $\sqrt{1+s_* t^2}$ in place of $\sqrt{1+t^2}$ and K_H multiplied by $\sqrt{s_*}$;

(iii) *there is $H \in \mathcal{N}_{\pi_{\mathbf{q}}}$ with $H(I_t^+) = 1$ and $H(I_t^-) = -1$ for all $0 < t < t_0$.*

Consequently

$$\inf_{H \in \mathcal{N}_{\pi_{\mathbf{q}}}} \sup_{0<t<t_0} R_t(H) = 0, \qquad \inf_{H \in \mathcal{N}_{\pi}} \sup_{0<t<t_0} R_t(H) = 1 \qquad (\pi = \pi_{\mathbf{1}},\ \pi_{\mathbf{1}} \circ \nu),$$

the second infimum being attained by $H = 0$; for the logistic loss the two infima are 0 and $\log 2$.

Proof. (i) is Thm. 7.5 below.

(ii) At p_0 a classifier with normalization $\pi_{\mathbf{1}}$ reads

$$v_t^{\pm} = \pi_{\mathbf{1}}(tu_1, \pm t^2 u_2, 0) = \frac{(u_1, \pm t u_2, 0)}{\sqrt{1+t^2}}, \qquad \|v_t^+ - v_t^-\| = \frac{2t}{\sqrt{1+t^2}}.$$

The two jets have the same block norms at every probe and the two images have the same intensity frame and mass, so by (P2) their weights, memberships and masses coincide, and every probe other than p_0 contributes the same value of ψ. In each weighted mean the coefficient of p_0 is at most one, also when $\eta > 0$. If L_ψ is a Lipschitz constant of ψ, each Φ_b changes by at most $L_\psi \|v_t^+ - v_t^-\|$, and the pooled vector by at most $\sqrt{B}\, L_\psi \|v_t^+ - v_t^-\|$. By (P1) the pooled vectors lie in a bounded set, on which Ω has a Lipschitz constant L_Ω by (P3); this gives the first bound with $K_H = L_\Omega \sqrt{B}\, L_\psi$. Write the two scores as $m \pm d$. Then $R_t(H) = m^2 + (d-1)^2$ with $|d| \le K_H t/\sqrt{1+t^2}$, which gives the second bound, and the convexity of $\ell(z) = \log(1+e^z)$ gives $C_t(H) = \frac{1}{2}\{\ell(-m-d) + \ell(m-d)\} \ge \ell(-d)$, which gives the third. For $\pi_{\mathbf{1}} \circ \nu$ the inputs at p_0 are $(u_1, \pm\sqrt{s_*}\, t u_2, 0)/\sqrt{1+s_* t^2}$, and the argument is the same.

(iii) At p_0, $\rho_{\mathbf{q}}(tu_1, \pm t^2 u_2, 0)^2 = \|tu_1\|^2 + \|t^2 u_2\| = 2t^2$ and

$$\pi_{\mathbf{q}}(tu_1, \pm t^2 u_2, 0) = \Big(\frac{u_1}{\sqrt{2}}, \pm\frac{u_2}{2}, 0\Big),$$

two points independent of t. Take $w_p \equiv 1$, $\eta = 0$ and $\psi(v)$ the trace coordinate of the second block of v, which is bounded and Lipschitz and takes the values $\pm\frac{1}{2}$ at the two points. The other probes have fixed jets and the memberships are fixed by (i), so the pooled vectors $z_\pm = (\Phi(I_t^\pm), M(I_t^\pm))$ do not depend on t, and they differ in a bin in which p_0 has positive membership. The affine function $\Omega(z) = 2\langle z - (z_+ + z_-)/2,\, z_+ - z_-\rangle / \|z_+ - z_-\|^2$ sends $z_\pm$ to ± 1.

By (ii) every classifier in $\mathcal{N}_{\pi_{\mathbf{1}}}$ or $\mathcal{N}_{\pi_{\mathbf{1}} \circ \nu}$ has $\liminf_{t\to 0} R_t \ge 1$ and $\liminf_{t\to 0} C_t \ge \log 2$, and the zero classifier attains these values for every t. Replacing Ω in (iii) by $M\Omega$ gives the logistic loss $\log(1+e^{-M})$, which tends to 0 as $M \to \infty$. □

The minimization is over score functions, not estimators. Larger weights in a radial classifier change only K_H, so the bounds of (ii) hold for every radial classifier, and the separation concerns the supremum over t: it gives no positive gap at a fixed t, nor in expectation over a fixed law of t. It is a separation in squared loss, cross-entropy and margin, not in zero-one error, since a radial classifier with the scores $\pm t$ keeps the correct signs. The family is not a dilation orbit: the parameter t contracts one local jet by its derivative orders while the rest of the measured structure stays fixed.

Remark 7.3. With exact Gaussian jets at finitely many probes, GCN, UCN and SNT are probe classifiers with the normalizations $\pi_{\mathbf{q}}$, $\pi_{\mathbf{1}}$ and $\pi_{\mathbf{1}} \circ \nu$. Here ψ is the composition of the equivariant layers and the linear reduction, which is bounded and Lipschitz on the compact image of the normalization; the weights are the foreground gate, a function of block norms and scale, times $A(s)/s$, together with the thresholds of Sec. A.1; the memberships are those of the bins; and Ω is the layer normalization, with a positive regularizer in its denominator, followed by the perceptron. Moreover GCN realizes Thm. 7.2(iii). Set the slope of its foreground gate to zero, so that $g = \frac{1}{2}$, and retain one real channel of frequency zero equal to the trace coordinate of the second block, which the lift selects and the product layer passes on with zero product coefficients. A gate multiplies a real coordinate by a positive even function of it, so the retained feature is odd and takes opposite nonzero values at the two retracted points. Reduce it to one output coordinate and set another one identically to zero. The two pooled vectors $p_\pm$ share that zero coordinate and their masses; a layer normalization identifies them only if $p_+ = ap_- + b\mathbf{1}$ with $a > 0$, the zero coordinate forces $b = 0$, and a common positive mass forces $a = 1$. Two ReLU units of the perceptron then implement the affine separator, since $r = \mathrm{ReLU}(r) - \mathrm{ReLU}(-r)$. Unused channels and product coefficients are set to zero, so the number of parameters is unchanged.

7.3. **Construction of the separating images.** Images here are smooth functions on the plane, not pixel arrays, and the probes are exact Gaussian derivatives. Repeated readings are omitted, and the derivatives are written in the basis ∂^α, from which the harmonic coordinates differ by an invertible linear change of basis.

Lemma 7.4. *Let $B \subset \mathbb{R}^2$ be a nonempty open ball. The linear functionals on $C_c^\infty(B)$ consisting of all distinct Gaussian-jet readings*

$$h \longmapsto \partial^\alpha (g_{s_p} * h)(x_p), \qquad 1 \le |\alpha| \le 3,$$

together with $\int h$, $\int x_1 h$, $\int x_2 h$ and $\int |x|^2 h$, are linearly independent. Hence their joint map onto its finite-dimensional target is surjective.

Proof. The functionals are integrals against Gaussian derivatives and the four moment polynomials, all analytic on $\mathbb{R}^2$. A linear dependence on $C_c^\infty(B)$ would make a linear combination of these functions vanish on B, hence everywhere. Along every ray the Gaussian terms decay faster than any polynomial, so the polynomial part vanishes. Group the remaining terms by centre and variance; each group has the form $P_j(x)\exp(-|x - x_j|^2/(2s_j))$ with P_j a polynomial. Suppose that some group is nonzero, and choose a generic ray $x = rv$ on which every nonzero P_j restricts to a nonzero polynomial and centres with the same variance have distinct projections onto v. Among the nonzero groups take the largest variance, and among those the largest projected centre. After division by its Gaussian factor, all other terms decay exponentially relative to its polynomial as $r \to \infty$, a contradiction. Hence every P_j vanishes, and since at a fixed centre and variance distinct Gaussian derivatives have linearly independent Hermite polynomial factors, all coefficients vanish.

For an explicit right inverse, let φ_i be the kernels and moment functions, and choose $\chi \in C_c^\infty(B)$ nonnegative and positive on an open set. The matrix $A_{ij} = \int \chi \varphi_i \varphi_j \, dx$ is positive definite, and for prescribed readings v the function $h_v = \chi \sum_j (A^{-1}v)_j \varphi_j$ has exactly those readings. □

Lemma 7.5. *Let the probes contain $p_0 = (0, s_*)$ and let the memberships be as in Thm. 7.2. There are $t_0 > 0$ and $I_0, \zeta_1, \zeta_2 \in C_c^\infty(\mathbb{R}^2)$ such that the images $I_t^\pm = I_0 + t\zeta_1 \pm t^2\zeta_2$, $0 < t < t_0$, take values in $[0, 1]$ with minimum 0 and maximum 1, have the intensity mass, centroid and root-mean-square radius of I_0 and its jets at every probe $p \neq p_0$, and satisfy $\mathcal{J}_{p_0} I_t^\pm = (tu_1, \pm t^2 u_2, 0)$. Moreover p_0 has membership greater than 10^{-3} in some bin.*

Proof. Take two nonnegative smooth radial bumps, one supported just inside and one just outside the circle $|x| = \sqrt{2s_*}$. Since

$$\Delta\, g_{s_*}(x) = \Big(\frac{|x|^2}{s_*^2} - \frac{2}{s_*}\Big) g_{s_*}(x),$$

their Gaussian-smoothed Laplacians at the origin have opposite signs, and a positive linear combination of the two bumps has zero smoothed Laplacian there. Normalizing its maximum to one gives I_0. Radial

symmetry kills the orders one and three and makes the Hessian isotropic, so the whole 3-jet of positive order of I_0 at $(0, s_*)$ vanishes. For bumps close enough to the circle, the root-mean-square radius is close to $\sqrt{2s_*}$, so that p_0 has $r = 0$ and τ close to $-\frac{1}{2}\log 2$. In the bin with centre $(\frac{1}{2}, -\frac{1}{2})$ and widths 0.3 its membership then approaches

$$\frac{1}{2}\left(1 + \cos\left[\frac{\pi}{2}\sqrt{\left(\frac{1/2}{0.3}\right)^2 + \left(\frac{1/2 - (\log 2)/2}{0.3}\right)^2}\right]\right) > 0.03.$$

Choose an open ball B on which $\delta < I_0 < 1 - \delta$ for some $\delta > 0$. By Thm. 7.4 there are $\zeta_1, \zeta_2 \in C_c^\infty(B)$ whose four moments vanish, whose jets vanish at every probe $p \neq p_0$, and whose jets at p_0 are $\mathcal{J}_{p_0}\zeta_1 = (u_1, 0, 0)$ and $\mathcal{J}_{p_0}\zeta_2 = (0, u_2, 0)$. For t_0 small enough the images $I_t^\pm = I_0 + t\zeta_1 \pm t^2\zeta_2$ take values in $[0, 1]$; outside B they coincide with I_0, so they keep its minimum 0 and maximum 1 and the contrast normalization leaves them unchanged. The vanishing moments fix the intensity mass, centroid and root-mean-square radius, and the linearity of Gaussian differentiation gives the prescribed jets. □

7.4. **Continuous classifiers and regularization.**

Corollary 7.6. *Let $\mathcal{D} \subset \mathbb{R}^2$ be a compact canvas containing the supports of the images $I_t^\pm = I_0 + t\zeta_1 \pm t^2\zeta_2$ of Thm. 7.5, and regard an image as an element of $C(\mathcal{D})$ with the uniform norm. If a function $H : C(\mathcal{D}) \to \mathbb{R}$ is continuous at I_0, then*

$$\liminf_{t\downarrow 0} R_t(H) \geq 1, \qquad \liminf_{t\downarrow 0} C_t(H) \geq \log 2.$$

If H is L_H-Lipschitz on the family, then

$$R_t(H) \geq (1 - L_H\|\zeta_2\|_\infty t^2)_+^2, \qquad C_t(H) \geq \log\bigl(1 + \exp[-L_H\|\zeta_2\|_\infty t^2]\bigr).$$

This holds in particular for every convolutional network built from continuous convolutions, continuous activations, finite max or average pooling and normalizations with a positive regularizer in the denominator.

Proof. $I_t^\pm \to I_0$ uniformly, so continuity gives $H(I_t^+) - H(I_t^-) \to 0$, and the two-score inequalities in the proof of Thm. 7.2 give the limits. In the Lipschitz case $|H(I_t^+) - H(I_t^-)| \leq L_H\|I_t^+ - I_t^-\|_\infty = 2L_H\|\zeta_2\|_\infty t^2$. □

The labels have different limits along two paths to the same image I_0, so the ideal graded classifier is discontinuous at I_0. The corollary applies equally to a classifier that reads the exact Gaussian probes, which are continuous functionals of the image, and to a graded classifier with a regularized norm and without hard thresholds. Hard thresholds need not be continuous; the next proposition covers them.

Proposition 7.7. *Fix $\varepsilon > 0$ and let $\pi_{\mathbf{q},\varepsilon}$ be the retraction with the blockwise regularized norm*

$$\rho_{\mathbf{q},\varepsilon}(f)^2 = \sum_{k=1}^{3}\bigl(\|f_k\|^2 + \varepsilon^2\bigr)^{1/k}, \qquad (\pi_{\mathbf{q},\varepsilon} f)_k = \frac{f_k}{\rho_{\mathbf{q},\varepsilon}(f)^k},$$

which is the norm of the implementation (Sec. A.1). On the images of Thm. 7.2 put $r_\varepsilon(t)^2 = (t^2 + \varepsilon^2) + (t^4 + \varepsilon^2)^{1/2} + \varepsilon^{2/3}$. Every $H \in \mathcal{N}_{\pi_{\mathbf{q},\varepsilon}}$ satisfies

$$|H(I_t^+) - H(I_t^-)| \leq \frac{2K_H t^2}{r_\varepsilon(t)^2} \leq 2K_H\varepsilon^{-2/3}t^2,$$

hence $R_t(H) \geq (1 - a_t)_+^2$ and $C_t(H) \geq \log(1 + e^{-a_t})$ with $a_t = K_H t^2/r_\varepsilon(t)^2 \to 0$. The minimax squared and logistic losses of $\mathcal{N}_{\pi_{\mathbf{q},\varepsilon}}$ on the family are 1 and $\log 2$.

Proof. The two jets at p_0 have the common regularized norm $r_\varepsilon(t)$, so

$$\|\pi_{\mathbf{q},\varepsilon}(tu_1, t^2u_2, 0) - \pi_{\mathbf{q},\varepsilon}(tu_1, -t^2u_2, 0)\| = \frac{2t^2}{r_\varepsilon(t)^2} \leq 2\varepsilon^{-2/3}t^2.$$

Every block of a regularized retraction has norm at most one, so (P1) applies on a bounded set, and the rest is the proof of Thm. 7.2(ii): the weights, memberships and masses of the two images coincide, even where a threshold makes them jump as functions of t. □

Thm. 7.2, Thm. 7.6 and Thm. 7.7 prove Theorem D. The unregularized norm of the selected jet is $\rho_{\mathbf{q}} = \sqrt{2}\,t$, the regularized one is at least $\varepsilon^{1/3}$, and the two are comparable for t of order $\varepsilon^{1/3}$; we prove no advantage on a range of t bounded away from zero. What Thm. 7.2 isolates is the contribution of the fibre quotient: along the contraction the two classes converge to one image, every classifier continuous in the image and every radial classifier eventually confuses them, and the graded retraction sees two fixed jets for every t. The robustness measured in Sec. 8 arises away from this singular point.

8. Experiments

We test Theorem B and Theorem C on handwritten digits. Every comparison is between networks that differ only in the normalization of the jet; the architecture, the number of parameters, the training data, the schedule and the number of epochs are the same.

8.1. **Protocol.** The digits are MNIST images on a canvas of 29 pixels, or 57 pixels when they are enlarged or blurred, contrast normalized as in Sec. 2.4. A network is trained on 10,000 unscaled training digits and validated on 2,000 others, the first and the last digits of a random permutation of the MNIST training set; three permutations give three training splits. It is tested on the first 5,000 MNIST test digits, presented at the zooms 0.5, 0.7, 1, 1.4 and 2 [19]; blurred by a sampled Gaussian of standard deviation $\sigma_b \in \{0.5, 1, 1.5, 2\}$ input pixels and contrast normalized again; at half resolution, by an antialiased reduction and a bicubic enlargement; and at the zooms 0.5 and 2 with $\sigma_b = 1$. For the variance of the output along zoom orbits, 200 test digits are presented at eleven zooms, log-uniform in $[1/2, 2]$ and in $[1/\sqrt{2}, \sqrt{2}]$. No network sees a blurred digit in training.

We compare GCN with its twins UCN and SNT (Thms. 6.1 to 6.3), each with 21,950 parameters, and with an ordinary convolutional network with three convolutional layers, global average pooling and 22,826 parameters. The latter is applied to inputs rescaled about the canvas centre so that their intensity radius $\hat{\sigma}$ equals the median radius of the training digits, which gives it the global size invariance that the pooling frame gives the graded networks; we call it the size-normalized network. All networks are trained with Adam and a one-cycle schedule, with peak learning rate $2 \cdot 10^{-3}$, batch 64 and weight decay 10^{-4}, for 12 epochs (1,884 steps), and the checkpoint with the best validation accuracy is kept. GCN and its twins are trained on the three splits; the networks with exchanged gates and the size-normalized network are trained on split 1.

Two networks are compared on the same test digits by the exact two-sided McNemar test on the per-digit predictions [33], with the Holm adjustment [31] over the ten conditions of Tab. 4 within each split. The binomial standard error of an accuracy near 95% on 5,000 digits is 0.3 points.

The gradings and ablations of Tabs. 2 and 3 come from earlier runs on MNIST-Scale, digits rescaled by a factor uniform in $[0.3, 1]$ [20, 21] and tested on the official MNIST test digits, so that they do not reproduce the protocol of that benchmark. In these runs the validation digits followed the training digits in the permutation, the rescalings of the test digits depend on the training size, the per-digit predictions were not recorded, and each configuration was trained once; we interpret only differences of several points.

8.2. **Scale.** Fig. 1 (left) and Tab. 1 test Thm. 4.1 under zoom. The zooms 0.5 and 2 shift the ladder by two rungs, under which GCN and SNT are invariant (Thm. 6.5); the zooms 0.7 and 1.4 are not shifts of the ladder. Trained at the single scale 1, GCN keeps 95.4% and 96.0% at the zooms 0.5 and 2 on average, against 96.0% at the training scale, and loses about 2.7 points at 0.7 and 1.4; its lowest accuracy over the five zooms and three splits is 92.3%. The same network with equal grades loses 34 and 17 points at 0.5 and 2 on average, and up to 41 in one split; on split 1, at the zoom 0.5, GCN is right and UCN wrong on 2,046 digits, and the reverse holds on 47. Along the zoom orbits the mean variance of the softmax output is 0.017–0.024 for GCN and 0.093–0.144 for UCN, and the predicted label is constant along the orbit for 85–89% and 33–52% of the digits. This is the behaviour that

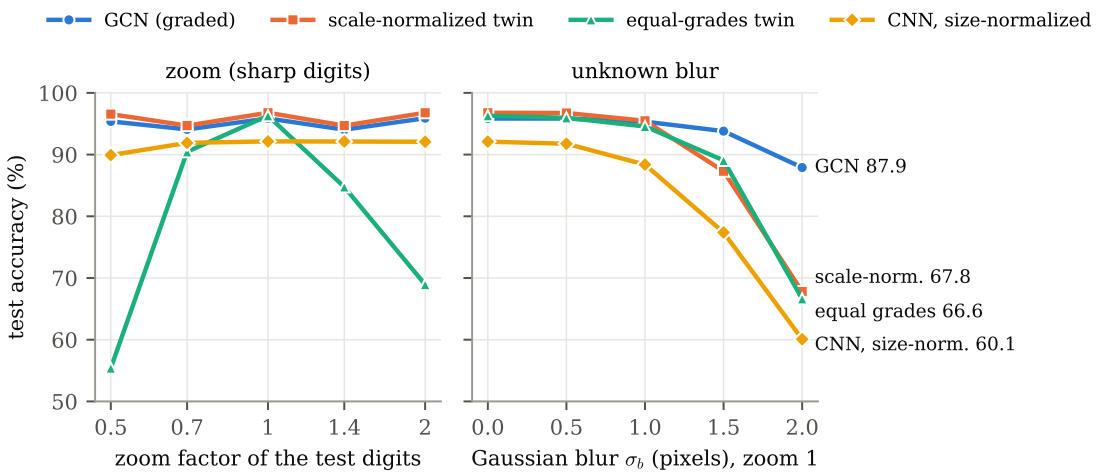


FIGURE 1. The graded network (GCN) against three baselines, all trained on 10,000 sharp unscaled MNIST digits and tested on 5,000 digits. Left: test digits zoomed by the factor shown. Right: test digits at their original size, blurred by a Gaussian of standard deviation σ_b pixels. The scale-normalized twin is the same network on scale-normalized derivatives, the equal-grades twin the same network with all grades equal, and the last baseline an ordinary convolutional network on inputs rescaled to a fixed size. Split 1; means over three splits in Tabs. 1 and 4.

Thms. 6.7 and 6.8 describe pointwise. Exchanging the foreground gates shows that the retraction, not the gate, carries the invariance: GCN with the gate of UCN is as flat as with its own, while UCN with the graded gate still loses 20 points at both shifts of the ladder.

TABLE 1. Zoom. Networks trained on 10,000 sharp unscaled digits, tested on 5,000 test digits resampled by the zoom factor: accuracy (%), mean variance of the softmax output over eleven zooms in $[1/2, 2]$ and in $[1/\sqrt{2}, \sqrt{2}]$ (200 digits), and percentage of digits whose predicted label is constant over $[1/2, 2]$. Upper block: mean ± half-range over three training splits; lower block: split 1. $\pi_{\mathbf{1}}$ is the radial projection, $\tilde{f} = s^{1/2} \star f$ the normalized jet.

Model	retr.	gate	0.5	0.7	1	1.4	2	var. $[\frac{1}{2}, 2]$	var. $[\frac{1}{\sqrt{2}}, \sqrt{2}]$	const.
GCN	$\pi_{\mathbf{q}}(f)$	$\rho_{\mathbf{q}}(\tilde{f})$	95.4±0.0	93.4±0.8	96.0±0.1	93.2±0.9	96.0±0.1	0.020±0.003	0.022±0.003	87±2
SNT	$\pi_{\mathbf{1}}(\tilde{f})$	$\|\tilde{f}\|$	96.2±0.4	94.5±0.3	96.8±0.2	94.5±0.4	96.8±0.2	0.019±0.002	0.018±0.003	89±1
UCN	$\pi_{\mathbf{1}}(f)$	$s^{1/2}\|f\|$	62.6±9.5	91.1±0.7	96.2±0.1	87.9±2.5	79.6±8.5	0.114±0.025	0.045±0.009	43±10
GCN, equal-grades gate	$\pi_{\mathbf{q}}(f)$	$s^{1/2}\|f\|$	95.5	94.3	95.9	94.1	95.9	0.017	0.018	89
UCN, graded gate	$\pi_{\mathbf{1}}(f)$	$\rho_{\mathbf{q}}(\tilde{f})$	76.1	91.6	96.5	89.6	76.3	0.090	0.042	52
CNN, size-normalized	–	–	89.9	91.9	92.1	92.1	92.1	0.004	0.002	93

The scale-normalized twin is invariant as well, as Thm. 4.1(i) predicts for the bundle quotient, and it is 0.8 to 1.3 points more accurate than GCN on average. The size-normalized network is flat across zooms, at 89.9–92.1%, about four points below GCN. Trained on MNIST-Scale, GCN reaches 95.6–95.7% in distribution and stays within 0.4 points of it at the zooms 0.5 and 2, while UCN, at 95.4–95.7% in distribution, falls to 81.9–85.5% at the zoom 2, which lies outside its training scales; SNT reaches 95.8–96.5% and is flat, and the size-normalized network reaches 86.96% in distribution and 88.1–88.4% at the five zooms (split 1). In the earlier runs, an ordinary convolutional network trained on unscaled digits reaches 94.9% at its training scale and 36.9% and 33.1% at the zooms 0.5

and 2; trained with scale augmentation by a factor log-uniform in $[\frac{1}{2}, 2]$ for five times the epochs, it reaches 92.8%, 75.4% and 86.1%, while GCN reaches 95.7%, 95.5% and 95.7% without augmentation.

Tab. 2 tests parts (iv) and (v) of Thm. 4.1. The gradings $(3,1,2)$ and $(1,3,2)$ are exactly invariant under their own action but not under the action of dilations. At the zoom 2, outside the training scales of MNIST-Scale, they keep 83.1% and 92.3%, against 95.5% for the correct grading and 82.2% for equal grades. A learnable grading $\boldsymbol{\theta} = e^{\boldsymbol{\varphi}}$ started at $(1,1,1)$, with the grade parameters at five and at twenty times the base learning rate, keeps 89.5% and 89.4%. Its grades move toward the ratios $1:2:3$ of the derivative orders, to $1:1.20:1.51$ and $1:1.22:1.49$ at the best-validation checkpoint, and stop short of them (Fig. 2).

TABLE 2. Gradings. Test accuracy (%) in distribution and at the zoom factors 0.5 and 2.0 (test digits resampled), and orbit variance in $[1/2, 2]$, for the correct, equal, wrong and learned gradings, all trained on MNIST-Scale. The learned gradings are those of the best-validation checkpoint, reported up to the common scale that leaves $\theta_1 = 1$.

Model	$\boldsymbol{\theta}$	test	zoom 0.5	zoom 2.0	orbit var.
GCN	$(1,2,3)$	95.3	95.7	95.5	0.0110
UCN	$(1,1,1)$	95.3	95.9	82.2	0.0338
wrong	$(3,1,2)$	93.8	94.1	83.1	0.0356
wrong	$(1,3,2)$	95.0	95.3	92.3	0.0246
learned	$(1.00, 1.20, 1.51)$	95.6	96.2	89.5	0.0217
learned, grade l.r. $\times 20$	$(1.00, 1.22, 1.49)$	95.7	96.3	89.4	0.0205

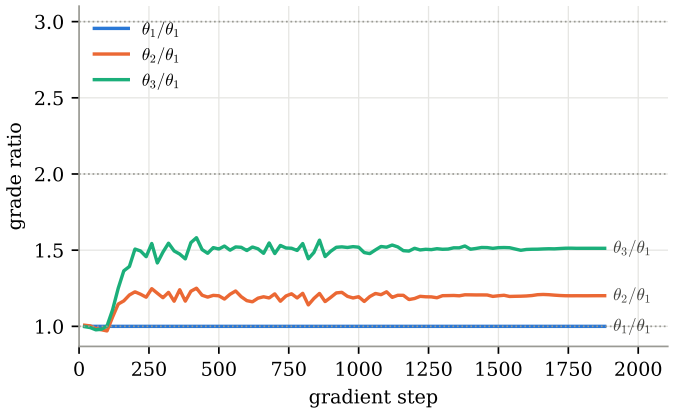


FIGURE 2. The ratios θ_k/θ_1 of the learnable grades during training, started at the equal grading $(1,1,1)$ with the grade learning rate at five times the base rate; the dotted lines are the ratios 1, 2, 3 of the derivative orders.

Tab. 3 reports ablations from the same earlier runs. The network on the 2-jet, with 15,702 parameters, reaches 94.3% in distribution, one point below the network on the 3-jet, and the network without the product layer, with 12,230 parameters, reaches 92.1%; both stay flat across zoom. With the invariant readout GCN is invariant under rotations by 90°, and nearly so at 30° and 60°, where interpolation enters, at a cost of 6.6 points in distribution; for upright digits the orientation carries class information.

8.3. **Unknown blur.** Fig. 1 (right) and Tab. 4 test Thm. 5.1 on the networks of Tab. 1, which were trained on sharp digits only. Averaged over the three splits, GCN loses 0.4 points at $\sigma_b = 1$, 2.1 at

TABLE 3. Ablations and rotation, trained on MNIST-Scale: test accuracy (%) in distribution, at zoom 2.0, and on the test digits rotated by 30°, 60°, 90°.

Model	test	zoom 2.0	30°	60°	90°
GCN, $N = 3$, full readout	95.3	95.5	71.7	24.8	12.2
GCN, $N = 2$	94.3	94.3	67.3	18.3	9.3
GCN, no product layer	92.1	92.5	67.7	22.6	11.7
GCN, invariant readout	88.7	87.1	86.1	86.1	87.1
UCN, full readout	95.3	82.2	66.6	15.7	8.5
UCN, invariant readout	88.1	51.1	81.6	81.7	81.9
CNN	89.1	32.0	40.8	8.8	7.4

$\sigma_b = 1.5$ and 7.6 at $\sigma_b = 2$. The scale-normalized twin, identical except for the normalization, loses 1.7, 9.8 and 30.6 points, and the equal-grades twin and the size-normalized network fall with it. At $\sigma_b = 2$, GCN is right and SNT wrong on 1,155, 1,394 and 1,166 digits in the three splits, and the reverse holds on 150, 107 and 132. Half-size digits blurred by one pixel, which model a smaller object seen through the same optics, give the same picture: 86.3% for GCN against 62.6% for SNT, 73.5% for UCN and 55.1% for the size-normalized network. After the Holm adjustment within each split, GCN is the more accurate at $\sigma_b = 1.5$, at $\sigma_b = 2$ and on the blurred half-size digits in all three splits ($p < 10^{-51}$), and at $\sigma_b = 1$ in two of them; SNT is the more accurate on sharp digits in all three, and under some of the mild conditions. At the zoom 2 a blur of one pixel is small compared with the enlarged strokes and changes nothing.

TABLE 4. Unknown blur. The networks of Tab. 1, trained on sharp digits and not retrained, tested on the same 5,000 test digits on the canvas 57: blurred by a Gaussian of standard deviation σ_b input pixels and contrast normalized again; with the resolution halved (antialiased reduction by two, bicubic enlargement); and at the zooms 0.5 and 2, sharp and with $\sigma_b = 1$. Accuracy in %, mean ± half-range over three training splits (the CNN: split 1). Last row: the number of splits in which GCN or SNT is the more accurate by the exact two-sided McNemar test on the same digits, Holm-adjusted over the ten conditions [31], at $p < 0.05$.

	zoom 1, blur σ_b					res.	zoom 0.5, σ_b		zoom 2, σ_b	
Model	0	0.5	1	1.5	2	$\times\frac{1}{2}$	0	1	0	1
GCN	96.0±0.2	95.9±0.1	95.6±0.2	93.9±0.3	88.4±0.5	95.4±0.1	95.4±0.0	86.3±1.4	96.0±0.1	95.9±0.2
SNT	96.8±0.2	96.7±0.2	95.1±0.4	87.0±0.3	66.2±2.7	96.0±0.4	96.2±0.4	62.6±3.1	96.8±0.2	96.6±0.3
UCN	96.2±0.1	96.0±0.1	94.9±0.4	90.7±1.4	76.0±7.1	95.1±0.1	62.6±9.5	73.5±3.6	79.6±8.5	77.9±9.6
CNN, size-norm.	92.1	91.8	88.4	77.4	60.1	89.9	89.9	55.1	92.1	91.7
more accurate	SNT 3/3	SNT 2/3	GCN 2/3	GCN 3/3	GCN 3/3	SNT 1/3	SNT 2/3	GCN 3/3	SNT 3/3	SNT 2/3

Tab. 5 separates the causes on split 1. Thm. 5.1(ii) holds exactly only without the second contrast normalization, which multiplies a blurred digit by $c_b = 1/\sup(g_b * I)$; over the first 2,000 test digits the median of c_b is 1.13, 1.37 and 1.66 at $\sigma_b = 1$, 1.5 and 2, and its maximum is 4.0. Without this normalization GCN keeps 88.5% at $\sigma_b = 2$ and 84.9% on the blurred half-size digits, slightly more than with it, while SNT keeps 64.7% and 59.5%. The contrast factor that the retraction keeps (Thm. 5.1(iii)) therefore does not limit GCN, and the one that the radial projection removes does not explain the failure of SNT. With the foreground gates exchanged, GCN with the gate of UCN keeps 88.0% and 84.8%, as with its own, while UCN with the graded gate of GCN falls to 64.5% and 72.7%, as with its own. The robustness is carried by the retraction. Its cause is the grading factor $\mu\star$ of Thm. 5.1(ii): with $\mu^2 = s/(s + b)$, the factor is far from one once the blur variance $b = 4\sigma_b^2$ working pixels^2 is comparable to the finest rung $s_0 = 2$, and on real digits a blur of 0.5 or 1 input pixel already changes the normalized jets by up to 24%, against at most 1.3% for the retracted jets (Sec. A.2).

TABLE 5. The mechanism of the blur robustness (split 1): accuracy (%) on the 5,000 test digits of Tab. 4, blurred by σ_b input pixels at zoom 1, and at the zooms $\frac{1}{2}$ and 2 with $\sigma_b = 1$. Without the second contrast normalization the jet of the blurred image is exactly the jet of the sharp image at the scale $s + b$ (Thm. 5.1); exchanging the foreground gates separates the retraction from the gate.

	zoom 1, blur σ_b					zoom, σ_b	
Model	0	0.5	1	1.5	2	$\frac{1}{2}$, 1	2, 1
without the second contrast normalization							
GCN	95.8	95.8	95.4	93.6	88.5	84.9	95.8
SNT	96.8	96.7	95.4	84.4	64.7	59.5	96.7
gates exchanged, contrast normalized as in Tab. 4							
GCN, equal-grades gate	95.9	96.0	95.5	93.6	88.0	84.8	95.9
UCN, graded gate	96.5	96.4	95.2	87.0	64.5	72.7	74.6

8.4. **Lindeberg's network.** The pooling of Sec. 6.2 does not use the grading, and it applies to any network that computes features on a ladder of scales. We apply it to our reimplementation of Lindeberg's Gaussian derivative network [9]: six layers of learned combinations of scale-normalized Gaussian derivatives, run in eight scale channels, with 20,674 parameters. The network is trained on 6,000 digits for six epochs with its binary cross-entropy loss, once with Lindeberg's maximum over the scale channels and once with our pooling, which weights the channels by their scale relative to the intensity radius of the image; nothing else changes. Tab. 6 uses two test sets: 800 test digits at sizes from $\frac{1}{2}$ to 4, and the first 2,000 of the blurred test digits of Tab. 4. The pooling makes the network invariant to zoom. On the first set, at half, twice and four times the training size, its accuracy rises from 69.3, 84.1 and 86.8% to 95.9, 98.0 and 97.5%, and the variance of its output over the sizes in $[1/\sqrt{2}, 2\sqrt{2}]$ falls from 0.122 to 0.003. Under blur at the training size both versions are robust, with 89.15 and 91.45% at $\sigma_b = 2$ on the second set; their later layers smooth further (Sec. 5.1). For the half-size digits of the second set the pooling is again decisive: 66.25 against 96.15% for sharp digits, and 73.35 against 83.65% for digits blurred by one pixel.

The networks with our pooling are then trained again with everything fixed except the first layer, which is graded. Its input, the scale-normalized 2-jet (f_1, f_2) of the image in each scale channel, is replaced by the retraction $(f_1/\rho,\ f_2/\rho^2)$ with $\rho = (\|f_1\|^2 + \|f_2\|)^{1/2}$, which is $\pi_{\mathbf{q}}$ for $N = 2$, and the four products of frequency zero $|z_1|^2$, $|h_2|^2$, h_0 and $\mathrm{Re}(\bar{h}_2 z_1^2)$ of the retracted jet (Sec. 2.2) are appended to it, which adds 48 parameters. The later layers are unchanged and remain scale-normalized. Since $\pi_{\mathbf{q}} \circ \nu = \pi_{\mathbf{q}}$ (Thm. 4.1(iii)), the graded first layer does not depend on the nominal scale, and by Thm. 5.1(ii) and (iii) a blur changes its input only by the change of scale $s \mapsto s + b$ and by the contrast factor of the second normalization.

In the paired counts below the first number counts the digits on which the first network is right and the second wrong, and the second number the reverse; the p-values are Holm-adjusted over the six conditions of Tab. 6. On sharp digits, under blurs up to $\sigma_b = 1.5$ and at the zoom $\frac{1}{2}$ the graded and the ungraded network are equally accurate, with no significant difference. Under the stronger blurs the graded network is more accurate: 93.10 against 91.45% at $\sigma_b = 2$ (85 against 52 digits, $p = 0.03$), and 89.75 against 83.65% for half-size digits blurred by one pixel (181 against 59, $p < 10^{-14}$). The comparison replicates in a second version of the network with the four scale channels $\sigma_0 \in \{2^{-1/2}, 2^{1/2}, 2^{3/2}, 2^{5/2}\}$ in place of eight, trained in the same way: 92.50 against 90.50% at $\sigma_b = 2$ (93 against 53, $p = 0.006$) and 88.35 against 82.25% for half-size digits blurred by one pixel (215 against 93, $p < 10^{-10}$), with no other significant difference. On the size test the grading changes the accuracy in neither version beyond the sampling error of 800 digits, and the variance of the output across sizes, 0.004 and 0.009, stays far below the 0.122 of the maximum over channels. Each network was trained once, on the same training digits, so the two versions replicate the comparison across architectures,

not across training data, and the paired tests account for the variation over test digits, not for that between training runs.

The gain comes from the retraction. A third version with eight scale channels retracts the jet of the first layer without appending the products, and so has exactly the parameters of the ungraded network. It is the most robust of all: 97.30, 95.10 and 91.45% at $\sigma_b = 1.5$, at $\sigma_b = 2$ and for half-size digits blurred by one pixel, against 96.10, 91.45 and 83.65% for the ungraded network (45 against 21, 104 against 31 and 200 against 44 digits; $p = 0.017$, $p < 10^{-8}$ and $p < 10^{-23}$), with no significant difference on sharp digits, at $\sigma_b = 1$ or at half size. The products lower the gain slightly: against the retraction alone, the first layer with products is right and the other wrong on 37 digits against 77 at $\sigma_b = 2$ ($p = 0.001$), and on 65 against 99 for the blurred half-size digits ($p = 0.049$).

TABLE 6. Lindeberg's Gaussian derivative network [9] in our reimplementation, in versions with eight and with four scale channels, each trained once with the same architecture, the same 6,000 digits at size 1, six epochs and the same loss. The pooling is Lindeberg's maximum over the scale channels or the image-frame pooling of Sec. 6.2; the graded first layer retracts the scale-normalized 2-jet and appends its four frequency-zero products (20,722 parameters against 20,674), and the retraction-only version retracts it without the products (20,674 parameters) (Sec. 8.4). Upper panel: accuracy (%) on 800 test digits at the sizes shown (canvas 113 above $\sqrt{2}$) and mean variance of the normalized outputs over the nine sizes in $[1/\sqrt{2}, 2\sqrt{2}]$. Middle panel: accuracy (%) on a second test set, the first 2,000 test digits of Tab. 4, blurred by σ_b input pixels, and at the zoom $\frac{1}{2}$ sharp and with $\sigma_b = 1$; on 2,000 digits every accuracy is a multiple of 0.05 and is given exactly. Lower panel: the digits of the second set on which only the first or only the second network of each pair is right, and the exact two-sided McNemar test between them, Holm-adjusted over the six conditions [31].

Pooling	0.5	$\frac{1}{\sqrt{2}}$	1	$\sqrt{2}$	2	$2\sqrt{2}$	4	var.
eight scale channels								
maximum over channels [9]	69.3	96.6	98.0	91.4	84.1	81.6	86.8	0.122
image-frame pooling	95.9	98.1	98.5	98.5	98.0	97.9	97.5	0.003
image-frame pooling, graded first layer	96.8	98.3	98.8	98.8	98.8	98.1	98.1	0.004
image-frame pooling, retraction only	96.4	98.9	98.6	98.5	97.9	97.8	97.9	0.004
four scale channels								
image-frame pooling	96.4	98.1	98.6	98.3	99.1	98.4	97.6	0.005
image-frame pooling, graded first layer	96.6	98.0	98.4	98.5	97.9	97.8	97.4	0.009

	blur σ_b, zoom 1				zoom, σ_b	
Pooling	0	1	1.5	2	$\frac{1}{2}$, 0	$\frac{1}{2}$, 1
eight scale channels						
maximum over channels [9]	97.60	96.70	94.80	89.15	66.25	73.35
image-frame pooling	98.45	98.05	96.10	91.45	96.15	83.65
image-frame pooling, graded first layer	98.25	97.85	96.60	93.10	96.25	89.75
image-frame pooling, retraction only	98.15	98.20	97.30	95.10	96.45	91.45
four scale channels						
image-frame pooling	98.20	97.95	96.50	90.50	96.90	82.25
image-frame pooling, graded first layer	98.20	97.50	96.15	92.50	96.50	88.35
eight scale channels						
graded vs. ungraded, digits right only for each	10/14	15/19	35/25	85/52	32/30	181/59
graded vs. ungraded, p (Holm)	1.00	1.00	0.98	0.030	1.00	$8 \cdot 10^{-15}$
retraction only vs. ungraded, digits right only for each	8/14	16/13	45/21	104/31	31/25	200/44
retraction only vs. ungraded, p (Holm)	0.86	1.00	0.017	$1 \cdot 10^{-9}$	1.00	$4 \cdot 10^{-24}$
graded vs. retraction only, digits right only for each	14/12	15/22	21/35	37/77	29/33	65/99
graded vs. retraction only, p (Holm)	1.00	0.97	0.33	0.001	1.00	0.049
four scale channels						
graded vs. ungraded, digits right only for each	12/12	8/17	29/36	93/53	25/33	215/93
graded vs. ungraded, p (Holm)	1.00	0.43	1.00	0.006	1.00	$2 \cdot 10^{-11}$

Lindeberg's network differs from GCN in depth, training data, number of epochs and loss, so these numbers concern the pooling and the grading within that architecture and do not compare the two

architectures. Under its own protocol the ungraded version is as robust to blur at the training size as GCN, with 89.15% against 88.90% at $\sigma_b = 2$ on the same 2,000 digits, and more accurate on sharp digits. In both architectures the retraction supplies the robustness to blur that scale normalization lacks: by a wide margin in the shallow network of Sec. 8.3, where no later smoothing compensates, and by a smaller but significant one in Lindeberg's deeper network, whose later layers compensate in part.

9. Conclusion

Derivative order grades the Gaussian jet of an image, and invariance under dilations forces this grading: every invariant local feature factors through the scale-normalized jet or, if it does not use the scale, through the retraction onto the weighted sphere of the grading. The two realizations differ under an unknown blur, which the retraction converts into a change of scale and the normalized jet into a residual grading factor, and at the singular point of the retraction the graded quotient separates local structures that no continuous classifier separates. Networks built on the retraction inherit these properties. On MNIST they are invariant to zoom and far more robust to blur than the same networks on scale-normalized derivatives, and the retraction alone, applied in the first layer of Lindeberg's Gaussian derivative network, makes that network more robust to blur as well.

The scale-normalized network is more accurate than GCN on sharp images, by 0.8 to 1.3 points on average over the three splits and by up to 2.6 in one, by up to 0.9 points on MNIST-Scale, and under mild blur ($\sigma_b \leq 0.5$, or the resolution halved). A possible cause, which we have not tested, is the conditioning of the retraction near vanishing blocks, where it is only Hölder continuous (Thm. 2.3). The invariance of the pooled features is exact for the even shifts of the ladder and not for continuous zoom. By Thm. 5.1 the grading factor that affects the scale-normalized network is largest at the finest rungs, where $\mu^2 = s/(s+b)$ is farthest from one; a scale-normalized network whose ladder starts at a coarser scale would be less sensitive to a blur of a given size, at the price of the fine scales that resolve the strokes, and we have not trained such a network. Deeper networks on scale-normalized derivatives, such as Lindeberg's, recover much of the robustness through their later layers, and retracting their first layer adds to it. Training with blur augmentation could supply part of the robustness, as scale augmentation supplies part of the scale invariance; GCN needs neither.

The experiments use one dataset of isolated, centred digits, three training splits for the shallow networks and one training run for each version of Lindeberg's network, and a Gaussian model of blur. Real defocus is not Gaussian, and invariants to Gaussian blur in the sense of [28, 30] are a different and complementary tool. The pooling uses a global intensity frame, which isolated digits provide; images with several objects or with clutter are not tested, and neither are the scale-equivariant networks with learned filters [19, 20]. It remains to test the graded retraction on other data, on images with clutter and under real optical blur.

Appendix A. Discretization and numerical verification

A.1. **Discretization.** Images are placed on odd square canvases, of 29 pixels for MNIST and 57 for images enlarged beyond the canvas, and upsampled by two with bicubic interpolation aligned at the corners, so that pixel x of the input is pixel $2x$ of the working grid. The ladder $s \in \{2, 4, \dots, 4096\}$ in working pixels^2, twelve rungs one octave of s apart, corresponds to $\sigma = \sqrt{s}/2 \in \{0.71, 1, 1.41, \dots, 32\}$ input pixels; the coarse rungs cost almost nothing and give the bins room on both sides. The Gaussian derivatives are separable sampled kernels truncated at $4\sqrt{s}$, in the cross-correlation form $K_a(t) = (\partial^a g_s)(-t)$. The jet at the rung s_i is sampled on a pyramid with stride $2^{\lfloor i/2 \rfloor + 1}$ working pixels, that is $2, 2, 4, 4, \dots, 64, 64$, on the grid $x = c + \text{stride} \cdot t$ through the canvas centre c. This grid is symmetric under the rotations by 90° and nests exactly under the dilation by two from the canvas C to the canvas $2C - 1$. A dilation by $\sqrt{2}$ shifts the ladder by one rung but resamples the pyramid, so the exact statements of Thm. 6.5(iii) are for even shifts. Positions whose foreground gate is at most 0.02, or whose bin memberships sum to at most 10^{-3}, are skipped; since g and m_b are invariant, so is the skipped set, but the selection is discontinuous where a threshold is crossed. The homogeneous norm uses $\|f_k\|^2 + \varepsilon^2$ with $\varepsilon = 10^{-12}$, so that the exactly flat background is mapped to zero, and it is

computed in the log domain, $\log \rho_{\boldsymbol{\theta}} = \frac{1}{2}\,\mathrm{logsumexp}_k\big(\frac{2}{\theta_k}\log\|f_k\|\big)$. For SNT the harmonic coordinates of order k are multiplied by $s^{k/2}$ before the radial projection. One epoch of 10^4 images takes about 35 seconds on two CPU cores.

A.2. **Numerical verification.** The statements of Secs. 2 to 5 and of Thm. 6.8 were checked with the scripts `verify_identities`, `verify_blur` and `verify_v6` of the code [34]. Symbolically: the statements of Thm. 4.1, together with the realizability of the jets of order at most 3 (the Gram matrix of the Gaussian derivatives of order at most 3 has full rank); Thm. 5.1 and the example that follows it; the two identities of Thm. 5.2 on polynomial images, for which the jet is finite; and the identities of Sec. 2.2 and of the transvectant $(f_2, f_2)^{(2)}$. Numerically, for Thm. 6.8: the activation pattern of a random ReLU network is constant beyond a computable μ_0, where the network equals its cubic exactly, and the radially projected network converges at the rate μ^{-1}. On real digits the sampled jets follow Sec. 5 up to discretization: for blurs of 0.5 and 1 input pixel, between the blurred digit at $s \in \{4, 8, 16\}$ working pixels^2 and the sharp digit at $s + b$, the retracted jets agree to 0.2–1.3% of their size, the sampled Gaussian not being an exact semigroup, while the radial projections of the normalized jets differ by 2–24%, most at the finest rung.

The equivariance statements were verified numerically (Tab. 7). The position features are invariant under their own grading action to 10^{-15}, and under the exact dilation by two of real digits the features of GCN at rung $i + 2$ agree with those at rung i to 0.01–0.24 standard deviations across digits, those of SNT to at most 0.08, while those of UCN differ by up to 1.86. Between $s = 4$ and $s' = 6$ working pixels^2 the normalized jet of order 0 and 1 of a digit changes by 13% and 20% of its size. The grading factor of Thm. 5.2 alone leaves 13% at order 0, where it is trivial, and overshoots to 33% at order 1; the grading factor and the heat correction, truncated at the 5-jet, leave 1% and 5%, which combine the discretization of the derivatives with the truncation of the heat series (E6).

TABLE 7. Numerical verification (`test_equivariance.py`); E3, E4 in double precision. Relative errors are maxima over random inputs or over 16–32 MNIST digits; "std" denotes standard deviations of the feature across digits. E1, E2, E5 and E6 measure the discretization of the image-level statements; only E3 and E4 are at machine precision.

Check	Result
E1 sampled Gaussian derivatives vs. the analytic jet of a blob, $s = 1, 2, 4, 8$	$3.9 \cdot 10^{-3}, 1.5 \cdot 10^{-3}, 3.6 \cdot 10^{-3}, 1.2 \cdot 10^{-3}$
E2 scale-space covariance (2) under D_2, analytic images, $s = 1, 2, 4$	$7.0 \cdot 10^{-5}, 1.2 \cdot 10^{-5}, 3.1 \cdot 10^{-5}$
E3 position features under $\mu\star_{\boldsymbol{\theta}}$ for $\boldsymbol{\theta} = (1, 2, 3)$ / $(1, 1, 1)$ / $(3, 1, 2)$	$1.5 \cdot 10^{-15}$/$1.1 \cdot 10^{-15}$/$1.3 \cdot 10^{-15}$
E3 features of $\boldsymbol{\theta} = (1, 1, 1)$ / $(3, 1, 2)$ under the dilation action $\mu\star_{\mathbf{q}}$	0.95 / 1.14
E4 harmonic coordinates transform by $e^{ij\phi}$; invariant readout rotation-invariant	$2.6 \cdot 10^{-16}$; $6.9 \cdot 10^{-16}$
E4 pooled vector, invariant readout, under exact 90° rotations of digits, GCN / UCN	$3.1 \cdot 10^{-14}$ / $1.3 \cdot 10^{-14}$
E5 per-rung features under D_2 of digits, rung $i + 2$ vs. i, ten rungs (std), GCN	0.24, 0.06, 0.05, 0.03, 0.04, 0.02, 0.02, 0.01, 0.03, 0.02
E5 same, UCN	1.86, 1.14, 0.70, 0.38, 0.28, 0.12, 0.08, 0.04, 0.85, 0.84
E5 same, wrong grading $(3, 1, 2)$	2.58, 0.95, 0.55, 0.21, 0.13, 0.06, 0.06, 0.03, 0.11, 0.06
E5 same, scale-normalized twin SNT	0.08, 0.07, 0.06, 0.03, 0.05, 0.02, 0.03, 0.01, 0.01, 0.00
E6 (8) on digits, $s = 4 \to 6$, order 0 / order 1: no correction, $\mu\star$ only, $\mu\star$ and heat	$1.3{\cdot}10^{-1}$, $1.3{\cdot}10^{-1}$, $9.8{\cdot}10^{-3}$ / $2.0{\cdot}10^{-1}$, $3.3{\cdot}10^{-1}$, $5.4 \cdot 10^{-2}$

DECLARATIONS

Funding. No funding was received for this work.

Competing interests. The author has no competing interests to declare.

Data availability. The MNIST digits are available from their original source and are not redistributed. The result files from which every table and figure of this paper is generated are openly available on Zenodo at https://doi.org/10.5281/zenodo.23997172 [34].

Code availability. The code and the trained networks are deposited with the result files [34], with instructions for regenerating each table from the stored results and for retraining every network.

References

[1] T. Shaska, *Graded neural networks*, Int. J. Data Sci. Math. Sci. **3** (2025), no. 2, 87–116, DOI 10.1142/S2810939225500030, available at arXiv:2502.17751. ↑1, 4, 5, 9, 10

[2] ———, *Artificial neural networks on graded vector spaces* (2024), preprint, available at arXiv:2407.19031. ↑1

[3] ———, *Graded transformers* (2025), preprint, available at arXiv:2507.20108. ↑1

[4] L. Hörmander, *The analysis of linear partial differential operators I: Distribution theory and Fourier analysis*, 2nd ed., Grundlehren der mathematischen Wissenschaften, vol. 256, Springer, 1990. ↑2, 5

[5] M. Felsberg and G. Sommer, *The monogenic signal*, IEEE Trans. Signal Process. **49** (2001), no. 12, 3136–3144. ↑6

[6] J. J. Koenderink, *The structure of images*, Biol. Cybernet. **50** (1984), 363–370. ↑2

[7] J. J. Koenderink and A. J. van Doorn, *Representation of local geometry in the visual system*, Biol. Cybernet. **55** (1987), 367–375. ↑2

[8] L. M. J. Florack, B. M. ter Haar Romeny, J. J. Koenderink, and M. A. Viergever, *Scale and the differential structure of images*, Image Vision Comput. **10** (1992), no. 6, 376–388. ↑2, 5

[9] T. Lindeberg, *Scale-covariant and scale-invariant Gaussian derivative networks*, J. Math. Imaging Vision **64** (2022), 223–242, available at arXiv:2011.14759. ↑1, 7, 21, 22

[10] Y. Jansson and T. Lindeberg, *Scale-invariant scale-channel networks: deep networks that generalise to previously unseen scales*, J. Math. Imaging Vision **64** (2022), 506–536. ↑1

[11] T. Lindeberg, *Feature detection with automatic scale selection*, Int. J. Comput. Vis. **30** (1998), no. 2, 79–116. ↑1, 3, 4, 6

[12] W. T. Freeman and E. H. Adelson, *The design and use of steerable filters*, IEEE Trans. Pattern Anal. Mach. Intell. **13** (1991), no. 9, 891–906. ↑3

[13] P. J. Olver, *Classical invariant theory*, London Mathematical Society Student Texts, vol. 44, Cambridge University Press, 1999. ↑10

[14] D. Hilbert, *Über die Theorie der algebraischen Formen*, Math. Ann. **36** (1890), 473–534. ↑12

[15] H. Derksen and G. Kemper, *Computational invariant theory*, 2nd ed., Encyclopaedia of Mathematical Sciences, vol. 130, Springer, 2015. ↑12

[16] G. Cybenko, *Approximation by superpositions of a sigmoidal function*, Math. Control Signals Systems **2** (1989), 303–314. ↑12

[17] M. Weiler and G. Cesa, *General $E(2)$-equivariant steerable CNNs*, Advances in Neural Information Processing Systems **32** (2019). ↑3

[18] A. Kanazawa, A. Sharma, and D. Jacobs, *Locally scale-invariant convolutional neural networks* (2014), preprint, available at arXiv:1412.5104. ↑2

[19] D. E. Worrall and M. Welling, *Deep scale-spaces: equivariance over scale*, Advances in Neural Information Processing Systems **32** (2019). ↑2, 11, 17, 23

[20] I. Sosnovik, M. Szmaja, and A. Smeulders, *Scale-equivariant steerable networks*, Int. Conf. Learning Representations (ICLR) (2020). ↑2, 11, 17, 23

[21] K. Sohn and H. Lee, *Learning invariant representations with local transformations*, Proc. 29th Int. Conf. Machine Learning (ICML) (2012), 1339–1346. ↑17

[22] B. Markussen, K. S. Pedersen, and M. Loog, *A scale invariant covariance structure on jet space*, Deep Structure, Singularities, and Computer Vision, Lecture Notes in Comput. Sci. **3753** (2005), 12–23, DOI 10.1007/11577812_2. ↑2

[23] ———, *Second order structure of scale-space measurements*, J. Math. Imaging Vision **31** (2008), 207–220, DOI 10.1007/s10851-008-0080-7. ↑2

[24] A. Perzanowski and T. Lindeberg, *Scale generalisation properties of extended scale-covariant and scale-invariant Gaussian derivative networks on image datasets with spatial scaling variations*, J. Math. Imaging Vision **67** (2025), no. 3, Paper No. 29, DOI 10.1007/s10851-025-01245-x. ↑1

[25] ———, *Scale-invariant Gaussian derivative residual networks* (2026), preprint, available at arXiv:2603.02843. ↑1

[26] E. Jenner and M. Weiler, *Steerable partial differential operators for equivariant neural networks*, Int. Conf. Learning Representations (ICLR) (2022), available at arXiv:2106.10163. ↑1, 2

[27] D. Yarotsky, *Universal approximations of invariant maps by neural networks*, Constr. Approx. **55** (2022), no. 1, 407–474, DOI 10.1007/s00365-021-09546-1. ↑1, 2, 11

[28] J. Flusser, S. Farokhi, C. Höschl IV, T. Suk, B. Zitová, and M. Pedone, *Recognition of images degraded by Gaussian blur*, IEEE Trans. Image Process. **25** (2016), no. 2, 790–806, DOI 10.1109/TIP.2015.2512108. ↑2, 23

[29] J. Kostková, J. Flusser, M. Lébl, and M. Pedone, *Handling Gaussian blur without deconvolution*, Pattern Recognit. **103** (2020), Paper No. 107264, DOI 10.1016/j.patcog.2020.107264. ↑2

[30] J. Flusser, M. Lébl, F. Šroubek, M. Pedone, and J. Kostková, *Blur invariants for image recognition*, Int. J. Comput. Vision **131** (2023), no. 9, 2298–2315, DOI 10.1007/s11263-023-01798-7. ↑2, 23

[31] S. Holm, *A simple sequentially rejective multiple test procedure*, Scand. J. Statist. **6** (1979), no. 2, 65–70. ↑17, 20, 22

[32] M. Leshno, V. Ya. Lin, A. Pinkus, and S. Schocken, *Multilayer feedforward networks with a nonpolynomial activation function can approximate any function*, Neural Networks **6** (1993), no. 6, 861–867, DOI 10.1016/S0893-6080(05)80131-5. ↑12

[33] Q. McNemar, *Note on the sampling error of the difference between correlated proportions or percentages*, Psychometrika **12** (1947), 153–157, DOI 10.1007/BF02295996. ↑17

[34] T. Shaska, *Code and results for "Graded convolutional networks: scale invariance without the scale and robustness to unknown blur"*, 2026. Zenodo. ↑3, 24, 25

Department of Computer Science & Engineering, Oakland University, Rochester, MI 48309
Email address: shaska@oakland.edu